Dalton Transactions

ROYAL SOCIETY OF CHEMISTRY

PAPER

View Article Online
View Journal | View Issue

Cite this: *Dalton Trans.*, 2022, **51**, 15049

Sterically demanding pyridine-quinoline anchoring ligands as building blocks for copper(I)-based dye-sensitized solar cell (DSSC) complexes†

Anastasios Peppas,[a] Demetrios Sokalis,[a] Dorothea Perganti,[b] Gregor Schnakenburg,[c] Polycarpos Falaras *[b] and Athanassios I. Philippopoulos *[a]

The Pfitzinger condensation reaction was employed to synthesise N^N sterically demanding ligands bearing carboxylic acid anchoring groups, namely 2,2′-pyridyl-quinoline-4-carboxylic acid (**pqca**), 6′-methyl-2,2′-pyridyl-quinoline-4-carboxylic acid (**6′-Mepqca**), 8-methyl-2,2′-pyridyl-quinoline-4-carboxylic acid (**8-Mepqca**) and 8,6′-dimethyl-2,2′-pyridyl-quinoline-4-carboxylic acid (**8,6′-Me$_2$pqca**). Preparation of the methyl ester analogues **6′-Mepqcame**, **8-Mepqcame** and **8,6′-Me$_2$pqcame** is also described. All ligands were fully characterised including the X-ray structures of **pqca**, **6′-Mepqca** and **8-Mepqca**. We also describe the synthesis and characterisation of seven homoleptic copper(I) complexes of the formula [Cu(N^N)$_2$][PF$_6$] (N^N = pqca (**1**), 6′-Mepqca (**2**), 8-Mepqca (**3**), 8,6′-Me$_2$pqca (**4**), 6′-Mepqcame (**6**), 8-Mepqcame (**7**) and 8,6′-Me$_2$pqcame (**8**)). Characterisation of the copper(I) complexes includes FT-IR, elemental analyses, multinuclear NMR spectroscopy, UV-vis spectroscopy, cyclic voltammetry, and a single-crystal X-ray diffraction study. The molecular structures of **1**·DMSO, 2{**2**·Me$_2$CO·0.5H$_2$O}, **4**, **6**·CHCl$_3$·0.13H$_2$O, 2{**7**·C$_5$H$_{12}$}·CHCl$_3$ and **8** have been determined, revealing that these complexes adopt a distorted tetrahedral geometry. These are the first crystallographically characterised examples of copper(I)-based coordination compounds incorporating the above mentioned N^N pyridyl-quinoline ligands. In solution, the new complexes are purple to red colored, while **2** displayed excellent stability in acetone at ambient temperature over a month. The absorption spectra of **1–8** display a main broad MLCT band with values of λ_{max} at ~530 nm and ε values ranging from 1800 to approximately 10 000 dm^3 mol^{-1} cm^{-1}. The photovoltaic performance of the prepared compounds was evaluated on mesoporous nanocrystalline TiO$_2$ dye-sensitized solar cells (DSSCs), and compared with that of the [Cu(dmdcbpy)$_2$][PF$_6$] dye (dmdcbpy = 6,6′-dimethyl-2,2′-bipyridine-4,4′-dicarboxylic acid) (**5**), that has been used as standard, under the same experimental conditions. From a combination of electrochemical and absorption spectroscopy experiments, the MLCT energy levels of **2** are appropriate for electron injection onto the titania conduction band. Upon optimisation of the semiconductor's architecture, **2** proved to be the most efficient dye, reaching a conversion efficiency of η = 1.20%, which is slightly higher than that of **5** (η = 1.05%), mainly attributed to higher V_{oc} values.

Received 21st July 2022,
Accepted 27th August 2022

DOI: 10.1039/d2dt02382b

rsc.li/dalton

Introduction

In the field of solar cells, pioneering studies by Grätzel and coworkers trace back to the early 1990s, leading to a landmark discovery with a power conversion efficiency of solar energy to electricity of approximately 10%.[1,2] This is a field of continuous interest, rendering dye sensitized solar cells (DSSCs) a realistic technology for harnessing the sun energy with power conversion efficiencies exceeding 12%.[3,4] To this end, a 14.3% efficiency has been recorded at the lab-scale,[5] denoting their potency as feasible alternatives to standard silicon-based solar cells.

In short, DSSCs consist of an n-type semiconductor electrode such as TiO$_2$ that is sensitized by dye molecules, with

[a]*Laboratory of Inorganic Chemistry, Department of Chemistry, National and Kapodistrian University of Athens, Panepistimiopolis Zografou 15771, Athens, Greece. E-mail: p.falaras@inn.demokritos.gr; Tel: +302107274697*
[b]*Institute of Nanoscience and Nanotechnology, National Center for Scientific Research "Demokritos", 15341 Agia Paraskevi, Attica, Greece. E-mail: atphilip@chem.uoa.gr*
[c]*Institut für Anorganische Chemie, Rheinische Friedrich-Wilhelms-Universität Bonn, Gerhard-Domagk-Straße 1, D-53121 Bonn, Germany*

† Electronic supplementary information (ESI) available: NMR and UV-vis spectra, cyclic voltammograms, crystal data, micro-Raman and IR spectra of the sensitized photoelectrodes. CCDC 2184654–2184660. For ESI and crystallographic data in CIF or other electronic format see DOI: **https://doi.org/10.1039/d2dt02382b**

the classical I^-/I_3^- redox mediator dissolved in a high boiling point nitrile or other solvent[6] along with the counter electrode, consisting of Pt nanoparticles.[7] The sensitization mechanism and the principles of cell operation have been well-established. At the heart of this device, an organic–inorganic dye, mainly a ruthenium(II) polypyridyl complex, is chemisorbed on the titania film.[8] Among the plethora of ruthenium dyes,[9,10] N719 (*cis*-$[Ru(dcbpyH_2)_2(NCS)_2][NBu_4]_2$, $dcbpyH_2$ = 2,2′-pyridine-4,4′-dicarboxylic acid) and Z907 constitute the state-of-the-art standard prototypes to comparatively evaluate the photoelectrochemical characteristics of a new molecular sensitizer.[11]

During the last decade, copper(I) complexes have emerged as alternatives to the standard ruthenium(II) dyes.[12] The low cost and high natural abundance of copper as compared with expensive ruthenium[13] constitute the basic reasons for this choice. In addition copper(I)-polypyridyl complexes display similar photochemical and photophysical properties[14] in comparison with ruthenium(II) congeners. The potential use of copper(I) with a carboxylate substituted 1,10-phenanthroline ligand in DSSCs has previously been reported by Sauvage and co-workers.[15] A substantial contribution to this topic has arisen from the seminal work of Housecroft, Constable and co-workers, with solar conversion efficiencies exceeding 2%.[13,16] In particular, for the synthesis of heteroleptic bis(diimine) copper(I) dyes this group has developed the 'surfaces-as-ligands, surfaces-as-complexes' approach,[17–19] while Odobel *et al.*, following the HETPHEN approach, have isolated a number of $[CuLL']^+$ dyes (L = anchoring, L′ = ancillary ligand),[20] with increased conversion efficiencies.[21] The progress of copper(I) complexes in light harvesting/energy conversion applications is highlighted in a recent review article.[22]

Given the continuous interest in copper(I) polypyridyl complexes that could be potentially applied in the field of DSSCs, we set up to synthesize new homoleptic copper(I) complexes incorporating appropriate sterically demanding anchoring ligands, to prevent geometric changes upon the oxidation of copper(I) to copper(II), which take place during the redox process.[12,23] The latter one is a prerequisite towards the design of copper(I)-based dyes. Following this strategy, we wanted to investigate the effect of varying the steric demands at the 6′ and 8-substituents within the class of 4-carboxy-2-(pyridin-2-yl)quinoline (**pqca**), on the performance of copper(I)-based DSSC devices. Well-described research on the ruthenium(II) coordination chemistry of **pqca** and its methyl ester analogue (**pqcame**) has provided us with the required knowledge to perform the current research.[24–26] Methylation at the 6′ and 8 positions of the anchoring ligand may act as a protecting scaffold for the copper(I) metal center. In this respect, stereochemical protection can be potentially offered by the benzo ring of the quinoline moiety, as was reported for $[Cu(^RDAB^{dipp})(L^{COOMe})][PF_6]$ ($^RDAB^{dipp}$ = 1,4-diaza-1,3-butadienes, R = H, Me; dipp = 2,6-diisopropylphenyl; L^{COOMe} = methyl-2-(pyridin-2-yl)-quinoline-4-carboxylate) complexes,[27] and for the case of a number of ruthenium(II) complexes.[15,28,29]

Accordingly, simple organic diimine ligand precursors, analogues of **pqca**, substituted with methyl at the 6′ (**6′-Mepqca**), the 8 (**8-Mepqca**), and both the 8 and 6′ positions (**8,6′-Me$_2$pqca**) of the pyridyl ring and the quinoline moiety, constitute the basis of this work. The synthesis of the methyl ester analogues **6′-Mepqcame**, **8-Mepqcame** and **8,6′-Me$_2$pqcame**, where the H atom of the COOH group was replaced by Me, is also reported. Herein, we focus on the preparation and characterisation of seven new homoleptic copper(I) dyes **1–4** and **6–8** of the type $[Cu(N^N)_2][PF_6]$, where N^N is one of the diimines reported above (N^N = pqca (**1**), 6′-Mepqca (**2**), 8-Mepqca (**3**), 8,6′-Me_2pqca (**4**), 6′-Mepqcame (**6**), 8-Mepqcame (**7**) and 8,6′-Me_2pqcame (**8**)), aiming to test them as molecular sensitizers for dye-sensitized solar cells. The $[Cu(dmdcbpy)_2][PF_6]$ dye (**5**), where dmdcbpy stands for 6,6′-dimethyl-2,2′-bipyridine-4,4′-dicarboxylic acid, was prepared independently in a one-pot reaction, serving as a copper(I) DSSC prototype for comparison of the performance of the device.[12]

Results and discussion

Synthesis and spectroscopic and structural characterisation of sterically demanding anchoring ligands

The 4-carboxy-2-(pyridin-2-yl)quinoline (**pqca**) precursor was prepared with slight modifications of the published procedure, following the Pfitzinger condensation reaction of isatin with 2-acetyl-pyridine, in a refluxing ethanol and aqueous KOH mixture.[30] According to this strategy, we extend the series of pyridyl-quinoline derivatives to the sterically demanding compounds **6′-Mepqca**, **8-Mepqca** and **8,6′-Me$_2$pqca** bearing methyl groups at the pyridyl ring, the quinoline moiety or both rings (Scheme 1).[31] Although the synthesis of the **8-Mepqca** ligand has already been reported,[32] in this study we present a complete spectroscopic characterisation, along with the crystal structure determination of this compound (*vide infra*).

The new organic precursors were obtained in high yields, as easily tractable materials that can be prepared on a gram scale in a one-pot procedure. They can be handled in air and stored

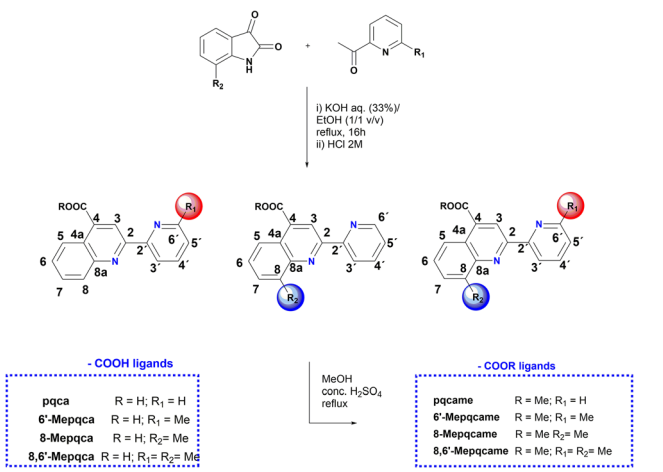

Scheme 1 Synthesis of the N^N anchoring ligands containing COOH groups and their methyl ester analogues.

for months without decomposition, showing high thermal stability, and decompose in temperatures ranging from 218 °C to 295 °C. Their solubility in most common organic solvents is poor; however, **8,6′-Me$_2$pqca** dissolves in Me_2CO, methanol and DMSO. The FT-IR spectrum of the precursors is dominated by the asymmetric stretching vibration mode of the C=O bond at approximately 1690 cm^{-1},[31,33] along with typical absorption bands for the C=C and C=N vibration modes, in the region of 1590–1450 cm^{-1}.[31] The ^{1}H and ^{13}C NMR spectra were in accord with the structures shown in Scheme 1; assignment was made with the help of ^{1}H–^{1}H COSY, ^{1}H–^{13}C HSQC and ^{1}H–^{13}C HMBC (ESI, Fig. S1–S9†) respectively. Within the series of ligand precursors, the singlet resonance signal of the methyl groups appear at δ 2.63 (**6′-Mepqca**), δ 2.8 (**8-Mepqca**) and δ 2.64, 2.87 ppm (**8,6′-Me$_2$pqca**) respectively.

The synthesis of the methyl ester analogues **6′-Mepqcame, 8-Mepqcame** and **8,6′-Me$_2$pqcame** is also reported; these generally display higher solubility in common organic solvents (Scheme 1). They were isolated as low melting solids (126 °C–154 °C), according to the improved synthesis reported for the **pqcame** ligand.[27] The ^{1}H NMR spectra of **6′-Mepqcame**, **8-Mepqcame** and **8,6′-Me$_2$pqcame** recorded in $CDCl_3$ are included in the ESI (Fig. S10–S18†), displaying the characteristic singlet resonance for the methyl group protons at δ 2.71 (6′-Me), 2.92 (8-Me) and 2.92/2.69 ppm (8,6′-Me) respectively. Assignment was based on a combination of ^{1}H–^{1}H COSY, ^{1}H–^{13}C HSQC and ^{1}H–^{13}C, HMBC.

Colorless single crystals of **pqca** and **6′-Mepqca**, suitable for X-ray diffraction, were grown upon slow evaporation of a DMSO solution of the compounds at ambient temperature. Low-quality yellowish needles, of **8-Mepqca**, were obtained upon crystallisation of complex **3** in a mixture of Me_2CO/Et_2O. Confirmation of the gross structural features of **8-Mepqca** was possible, despite the poor dataset refinement. As a result, we present only the molecular structure of this compound without describing its structural bonding parameters. Notably, a CSD search in the crystallographic data center revealed that the structures of these simple molecules had not previously been reported. Their molecular structures are depicted in Fig. 1–3.

As expected, the two nitrogen atoms about the biaryl bond adopt a *trans*-configuration.[13,16] **Pqca** crystallises in the monoclinic crystallographic system, $P2_1/n$ space group and **6′-Mepqca** in the orthorhombic, $P2_12_12_1$ space group. In **pqca** the pyridine ring close to the quinoline deviates from planarity, as the angle between the least-squares planes of the rings containing atoms N1 and N2 is 39.96°. For **6′-Mepqca**, however, this angle drops to 0.76°, indicating that the molecule is planar. The asymmetric unit of **pqca** contains four molecules that are stabilised by non-classical intermolecular hydrogen bonding interactions (distance of O2···H14–C14 = 2.884 Å, bond angle = 124.73°). The bonding parameters are in accord with those reported for the methyl 2-(2-pyridyl)quinoline-4-carboxylate, **pcame** analogue.[34]

The packing in the crystal of **6′-Mepqca** is such that a pair of molecules is stabilised by weak intermolecular π–π stacking

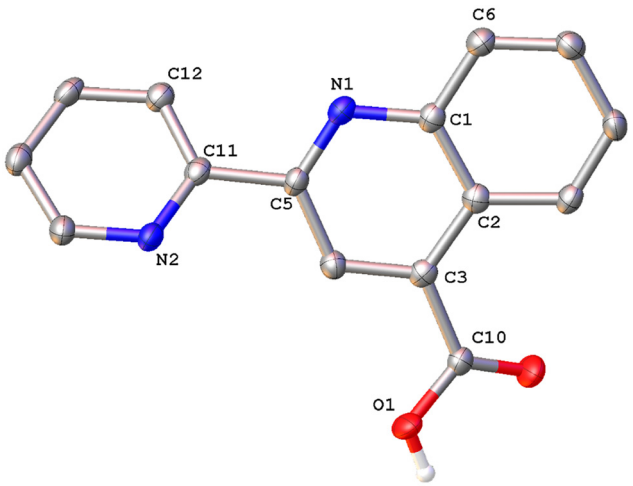

Fig. 1 Molecular structure of **pqca**; ellipsoids are plotted at the 50% probability level. H atoms except those in the COOH groups are omitted. Selected bond lengths (Å) and angles (°): O(1)–C(10) 1.317(3); O(2)–C(10) 1.214(3); N(1)–C(5) 1.311(4); N(2)–C(11) 1.337(4); C(5)–C(11) 1.503(4); C(5)–N(1)–C(1) 117.9(2); C(11)–N(2)–C(15) 118.5(2); O(2)–C(10)–O(1) 124.1(3).

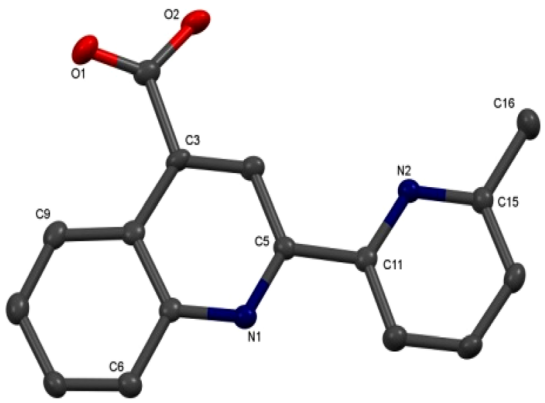

Fig. 2 Molecular structure of **6′-Mepqca**; ellipsoids are plotted at the 50% probability level. H atoms are omitted. Selected bond lengths (Å) and angles (°): O(1)–C(10) 1.216(4); O(2)–C(10) 1.322(4); N(1)–C(5) 1.329(4); N(2)–C(11) 1.353(4); C(5)–C(11) 1.492(4); C(15)–C(16) 1.496(4); C(5)–N(1)–C(1) 118.4(2); C(15)–N(2)–C(11) 118.7(2); O(1)–C(10)–O(2) 123.9(3).

interactions,[35] between the pyridine/quinoline and quinoline/phenyl rings (distance between centroids (N2–C11–C15)/(N1–C1–C5) and (N1–C1–C5)/(C1–C7–-C9) of 3.760 Å and 3.631 Å respectively) as shown in Fig. S19 of the ESI.† Lastly, a third molecule, almost orthogonal to this pair, displays typical intermolecular hydrogen bonding interactions *via* its N2 atom (distance of N2···H2–O2 = 1.911 Å, bond angle of 165.62°).[36]

Synthesis and characterisation of the homoleptic copper(I) complexes 1–4

The copper(I) complexes **1–4** were selectively prepared from the reaction of $[Cu(MeCN)_4][PF_6]$ with two molar equivalents of the appropriate ligand (**pqca**, **6′-Mepqca**, **8-Mepqca** and **8,6′-**

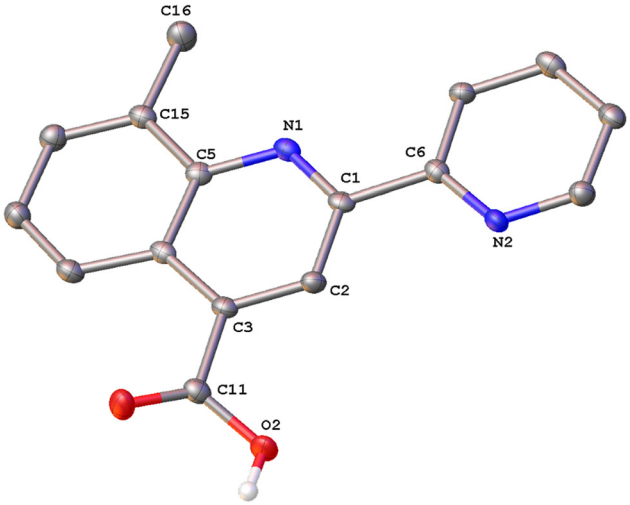

Fig. 3 Molecular structure of **8**-Mepqca; ellipsoids are plotted at the 50% probability level. H atoms, except those in the COOH groups are omitted.

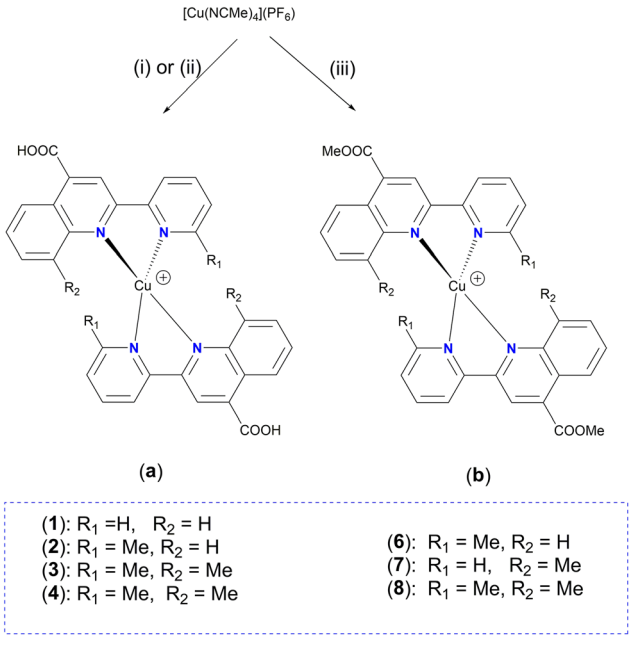

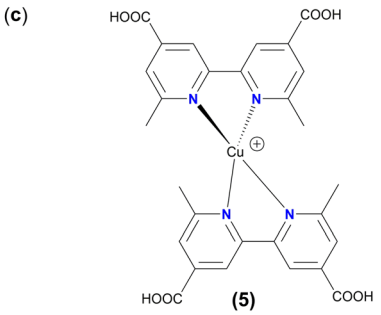

Scheme 2 Reaction scheme of the copper(I) cations of complexes **1–4** (a) and **6–8** (b); (i) pqca or 6′-Mepqca, DMSO; (ii) 8-Mepqca or 8,6′-Me_2pqca, Me_2CO; (iii) 6′-Mepqcame, 8-Mepqcame, 8,6′-Me_2pqcame, CH_2Cl_2. (c) Molecular structure of **5**.

Me_2pqca) at ambient temperature. The synthetic route and reaction conditions are depicted in Scheme 2a.

The poor solubility of the **pqca**, **6′-Mepqca**, **8-Mepqca** and **8,6′-Me_2pqca** ligands, incorporating a carboxylic acid anchoring group, in common organic solvents is a drawback for the one-pot preparation of the relevant homoleptic copper(I) dyes. In our approach we wanted to avoid the classic two-step synthesis that includes the reduction of copper sulfate with ascorbic acid under basic conditions, and subsequent acidification, which generally suffers from low synthetic yields and purification problems of the final product.[37]

We realized that in DMSO, a smooth, one-pot reaction occurs immediately, affording **1**·0.6DMSO and **2**·0.9DMSO as air- and moisture-stable purple-black powders, in 72% and 80% yields. The presence of co-crystallized DMSO is confirmed by NMR (^{1}H, ^{13}C) spectroscopy and by elemental analysis. Both complexes are thermally stable and decompose upon heating at temperatures higher than 206 °C and 182 °C. Initial attempts to prepare **3** following the route reported above were unsuccessful since an unknown grayish solid was obtained, accompanied by ligand elimination (ligand formation was proved by ^{1}H NMR spectroscopy, in solution). We then turned to acetone, where **3** was finally isolated as a black powder in 75% yield, which decomposes at 210 °C. Stability in this medium is rather limited and upon standing for approximately 20 min, precipitation of a black insoluble material was observed, and the color of the solution faded.

Solubility of **8,6′-Me_2pqca** in acetone is satisfactory, permitting the formation of complex **4** in quite high yield (>92%) as a dark red solid, which decomposes at 195 °C. Homoleptic complex **5** (Scheme 2c), bearing the dmdcbpy ligand, has previously been prepared in 27% yield.[12] Herein, we managed to isolate complex **5** in high yield (70%), according to the procedure reported for **1**·0.6DMSO and **2**·0.9DMSO. Our ^{1}H NMR and UV-vis spectroscopic data agree with those reported in the literature.[12]

The composition of the copper(I) complexes **1–4** was confirmed by elemental analyses, and spectroscopic characterisation was examined by FT-IR, UV-vis, and NMR spectroscopy (^{1}H–^{1}H COSY, ^{1}H–^{13}C HSQC and ^{1}H–^{13}C HMBC methods). The molecular composition of **1** and **2** was further confirmed by electro-spray mass spectral data, exhibiting peak envelopes corresponding to $[M - PF_6]^+$ and $[M + H]^+$ respectively, with the correct isotope pattern. The FT-IR spectra of **1–4** are almost identical from 4000 to 400 cm^{-1}, as expected for compounds that have similar molecular structures, indicating also successful coordination of the ligands.[25,26] All complexes exhibit the typical strong absorption for the ν_{as}(C=O) at ~1718–1707 cm^{-1}, indicating the presence of the carboxylic acid anchoring group in the corresponding ligands. This further suggests that the COOH group is not involved in coordination with the copper(I) centre. The very strong bands at

approximately 842 cm^{-1} and 558 cm^{-1} can be readily assigned to the ν_3(P–F) and ν_4(P–F) vibration modes of the PF_6^- anion.[38]

The ^1H and ^{13}C NMR spectra of **1**, **2**, **3** and **4** in Me_2CO-d_6, were assigned by 2D routine techniques (Fig. S20–S30†). The ^1H NMR spectra of **1** and **2** display sharp and well resolved peaks, attributed to the protons of **pqca** and **6′-Mepqca** ligands. The intense singlet resonance at δ 9.20 (**1**) and 9.22 ppm (**2**) is typical of the H3 proton of the quinoline ligand, which is uncoupled. Co-crystallized DMSO is verified by the singlet resonance at δ 2.67 (**1**) and 2.62 (**2**) ppm (see Fig. S20†). The ^{13}C NMR spectra of **1** and **2** are very informative, displaying typical resonance signals for carbon C6′, where the relevant hydrogen atom has been substituted by a methyl group. Ongoing from **1** (δ 150.3 ppm) to **2**, this resonance is shifted toward lower fields ($\Delta\delta \sim 9$ ppm). Moreover, for **2**, the singlet resonance at δ 41.1 ppm is attributed to the methyl carbon of co-crystallised DMSO. Notably, **2** proved to be very stable in Me_2CO-d_6 at ambient temperature, as its ^1H NMR spectrum remained unaltered for 36 days (Fig. S24b†). In contrast, the less constrained compound **1** was stable for a period of 14 days (Fig. S21†). The ^1H NMR spectrum of **3** (Fig. S27†) that was recorded at ambient temperature immediately after dissolution displays rather broad resonance signals, with an integration that is in accord with the proposed structure. The low stability of **3** in Me_2CO-d_6 solution did not permit us to record an appropriate ^{13}C NMR spectrum of this complex. The ^1H NMR spectrum of **4**, in Me_2CO-d_6, displays the expected resonance signals that are slightly broadened (Fig. S28†), implying that steric hindrance at the C6′ and C8 positions of the pyridine/quinoline rings is more effective. This is in accord with the structural features obtained from single-crystal crystallography. Analyzing the ^1H NMR spectrum of **4**, the singlet resonance at δ 9.02 ppm is attributed to H3, and the pseudo-triplet resonance at δ 8.26 ppm to proton H4′. Characteristics are the two high field signals at δ 2.71 and δ 2.14 ppm, assigned to the methyl groups of the quinoline and pyridine moieties, respectively.

Synthesis and characterisation of the copper(I) complexes 6–8

To stabilize the oxidation state around the copper(I) centre, electron-withdrawing substituents, such as methyl ester functionalities, have been considered. The homoleptic copper(I) complexes **6–8** (Scheme 2b), were prepared from the reaction of $[Cu(MeCN)_4][PF_6]$ with each of the methyl esters **6′-Mepqcame**, **8-Mepqcame** and **8,6′-Me$_2$pqcame** at ambient temperature in CH_2Cl_2. They are isolated as air-stable purple to red solids that dissolve better in common organic solvents than the acid congeners. The latter characteristic helped us to record well-resolved NMR spectra and characterise the new compounds appropriately. As a result, assignment of the NMR spectra of the less soluble complexes **2–4**, with carboxylic acids in their periphery, became possible. Complexes **6–8** were prepared aiming to test their possible application in a DSSC. In general, the electron-withdrawing character of the ester functionality may shift the characteristic MLCT absorption band towards the lower energies,[39] which may be beneficial for the performance of a DSSC.

The FT-IR spectra of **6–8** are characterised by a strong asymmetric stretching vibration typical of the ν_{as}(C=O) of the ester moiety at ~1730 cm^{-1}, shifted to higher wave numbers compared with **1–4**, which is in good agreement with the vibration mode reported for the $[Cu(pqcame)_2][PF_6]$ complex, at 1726 cm^{-1}.[27]

The NMR spectra of **6–8** were recorded in $CDCl_3$ and assignment was based on routine two-dimensional (2D) NMR techniques (ESI, Fig. S31–S39†).

X-ray

The solid-state structures of **1**·DMSO, $2\{2\cdot Me_2CO\cdot 0.5H_2O\}_2$, **4**, **6**·$CHCl_3$·$0.13H_2O$, $\{7\cdot C_5H_{12}\}_2\cdot CHCl_3$ and **8** were unambiguously determined by single-crystal X-ray diffraction. Suitable single crystals of **1**·DMSO were obtained by slow diffusion of pentane into an acetone solution of the compound, while crystals of **2**·Me_2CO·$0.5H_2O$ were grown from an acetone solution of **2** layered with n-hexane. Very low-quality red plates of **4** were isolated when diethyl ether was diffused into an acetone solution of the complex. Crystals of **6**·$CHCl_3$·$0.13H_2O$, $2\{7\cdot C_5H_{12}\}\cdot CHCl_3$ and **8** were obtained upon diffusion of pentane into a chloroform solution of the relevant complex (**6**, **7**, **8**), at ambient temperature.

The molecular structures of all cations of complexes are depicted in Fig. 4–8 and the bond parameters are listed in Table S1.† Hydrogen atoms, the PF_6^- anion and the co-crystallized solvents are omitted for clarity.

All complexes possess a four-coordinated copper(I) metal centre with coordination geometries varying from slightly distorted tetrahedral to that of a distorted tetrahedron. To quantify this distortion, the τ_4 geometry index introduced by Houser was employed.[40] In general, the values of τ_4 range from

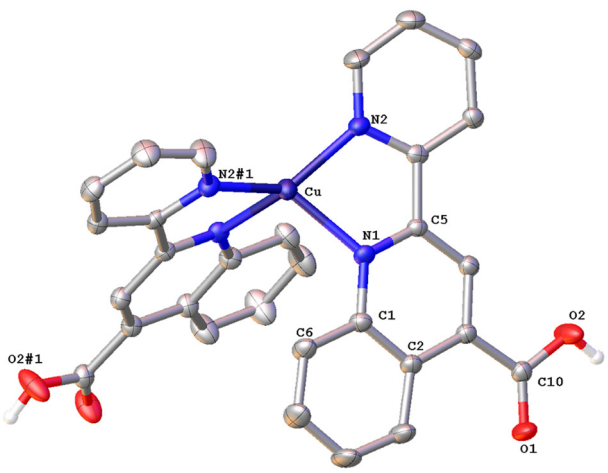

Fig. 4 Molecular structure of the cation of complex ([Cu(pqca)$_2$][PF_6]·DMSO (**1**·DMSO)); ellipsoids are plotted at the 50% probability level. H atoms, except those in the COOH groups, and the co-crystallized solvents are omitted for clarity.

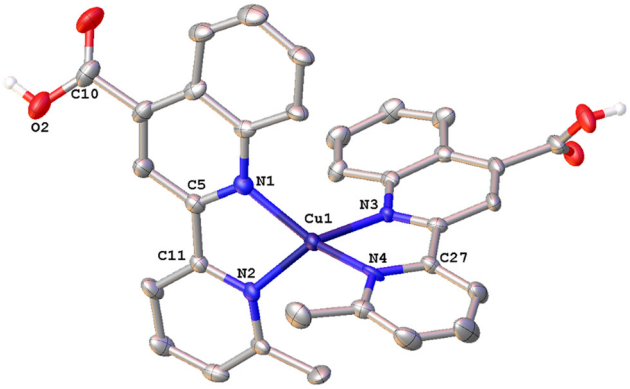

Fig. 5 Molecular structure of the cation of complex 2{[Cu(6′-Mepqca)$_2$][PF$_6$]·Me$_2$CO·0.5H$_2$O} (2{**2**·Me$_2$CO·0.5H$_2$O}); ellipsoids are plotted at the 50% probability level. H atoms, except those in the COOH groups, and the co-crystallized solvents are omitted for clarity.

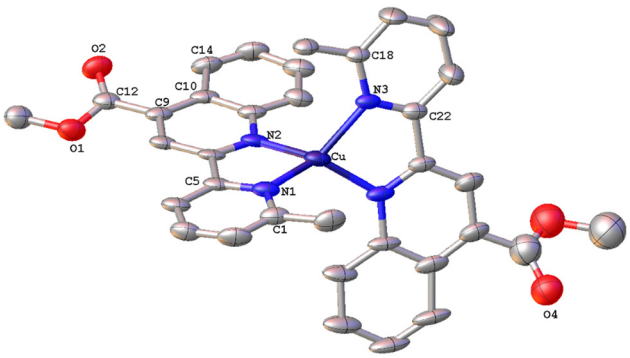

Fig. 6 Molecular structure of the cation of complex [Cu(6′-Mepqcame)$_2$][PF$_6$]·CHCl$_3$·0.13H$_2$O (**6**·CHCl$_3$·0.13H$_2$O); ellipsoids are plotted at the 30% probability level. H atoms, except those in the COOH groups, and the co-crystallized solvents are omitted for clarity.

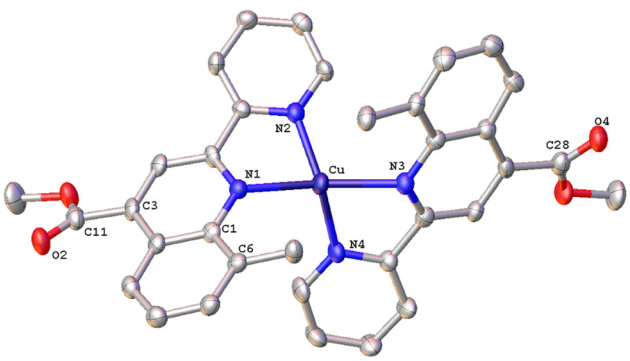

Fig. 7 Molecular structure of the cation of complex [Cu(8-Mepqcame)$_2$][PF$_6$] (2{**7**·C$_5$H$_{12}$}·CHCl$_3$); ellipsoids are plotted at the 50% probability level. H atoms, except those in the COOH groups, and the co-crystallized solvents are omitted for clarity.

1.00 (ideal tetrahedral geometry) to 0.00 (ideal square-planar geometry) and can be calculated by the formula $\tau_4 = [360 - (\alpha + \beta)]/141$, where α and β are the largest θ angles of a four-co-

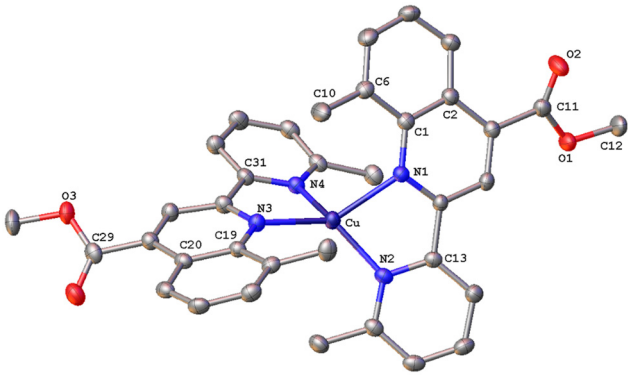

Fig. 8 Molecular structure of the cation of complex [Cu(8,6′-Me$_2$pqcame)$_2$][PF$_6$] (**8**); ellipsoids are plotted at the 50% probability level. H atoms, except those in the COOH groups, and the co-crystallized solvents are omitted for clarity.

ordinated complex. Accordingly, the calculated τ_4 values for complexes **1**, **2**, **6**, **7** and **8** range between 0.49–0.73, which is indicative of significant distortion from the ideal tetrahedral geometry. Our results compare well with the τ_4 values of 0.67 and 0.66 reported for $[Cu(L)(phen)]^+$ and $[Cu(L)(dmp)]^+$ (L = 6,6′-dimesityl-2,2′-bipyridine; dmp = 2,9-dimethyl-1,10-phenanthroline) respectively, where a distorted trigonal pyramidal geometry has been proposed.[41] This is also in good agreement with the reported τ_4 value of 0.59, for [Cu(pqcame)$_2$][PF$_6$],[27] albeit the new compounds are slightly less distorted. Notably, complex **7**, with a methyl group at the C8 of the quinoline ring, displays a geometry index τ_4 = 0.49 implying a severe distortion from the ideal tetrahedral geometry.

Complex **1**·DMSO (Fig. 4) adopts a distorted tetrahedral geometry. Flattening is confirmed by the dihedral angle of 55.34° between the two five-membered chelate rings including the copper(I) centre (Cu–N(1)–C(5)–C(11)–N(2)) and (Cu–N(1)–C(5)–C(11)–N(2)) respectively. This structural feature is in accord to the relative τ_4 index of 0.68, calculated above for this complex. In this conformation, the pyridine ring is twisted 13.35° out of the plane of the relative quinoline moiety that is bonded.

The angle between the least-squares planes of the pyridine and quinoline unit is 7.23°, as reported for other copper(I) complexes incorporating the 2-(pyridin-2-yl)quinoline moiety.[42] Also, the bite angle of the bipyridine unit is 81.21°, while other N–Cu–N bond angles are within the range of 102.58(15) to 132.70° (Table S1†). Complex **1**·DMSO exhibits characteristic C–H···π interactions (Fig. S40a†) between the H(15) hydrogen atom of the pyridine ring and the phenyl group centroid of quinoline, from an adjacent molecule (distance of (C15–H15)···centroid (ring (C6–C9)) = 3.549 Å.

In addition, the crystal packing in the structure of **1**·DMSO is such that symmetry-related molecules are separated by typical π–π stacking interactions, including the phenyl rings of the quinoline moieties from adjacent molecules, at a distance of 3.899 Å (view along the *a*-axis). Additional stabilization offers the non-classical hydrogen bonding between the aro-

matic hydrogen atom H(8) and the O(1) atom of the adjacent carbonyl group (C(8)–H(8)···O(1) = 2.543 Å, bond angle = 171.52°). To this end, the co-crystallized DMSO solvent molecules and the PF_6^- counter anions (in all directions) participate in extensive classical and non-classical hydrogen bonding interactions (Fig. S40b†).[36,43] Typical hydrogen bonds include the O(3) oxygen atom of DMSO and H(2) of the carboxylic acid group (O(2)–H(2)···O(3) = 1.813 Å, bond angle = 167.32°), while non-classical hydrogen bonding includes the F atoms of the PF_6^- counter anions and the hydrogen atoms of methyl groups from DMSO (C(16)–H(16A)···F(1)–P) = 2.829 (Å) as well as the aromatic hydrogen atoms of adjacent molecules. Bond lengths are in the range of 2.480–2.690 Å, as expected for other similar copper(I) polypyridine complexes.[42]

The asymmetric unit of 2{**2**·Me_2CO·0.5H_2O} (Fig. 5) consists of two crystallographically independent molecules (Cu1 and Cu1′) with marginally different bonding parameters. Both molecules reveal a distorted tetrahedral coordination geometry, as shown by the N(1)–Cu1–N(2), N(4)–Cu1–N(1) angles of 81.6(2)° and 135.2(2)° for the Cu1 atom, and N(3)′–Cu1′–N(2)′, N(4)′–Cu1′–N(2)′ angles of 81.2(2)° and 124.9(2)° for the Cu1′ atom, which differ from those of a perfect tetrahedron. In the crystal structure, it is clearly seen that the methyl group at the C6′ sufficiently protects the metal centre, leading to a less flattened structure (τ_4 = 0.71). This becomes evident from the dihedral angle of 83.41° between the planes of the five-membered chelate rings Cu(1)–N(1)–C(5)–C(11)–N(2) and Cu(1)–N(3)–C(21)–C(27)–N(4) and that of 85.07° between the planes Cu(1′)–N(1′)–C(5′)–C(11′)–N(2′) and Cu(1′)–N(3′)–C(21′)–C(27′)–N(4′), respectively. These angles are closer to 90°, as compared with that of **1**·DMSO (55.34°), and are in accordance with the literature reports.[16] In the asymmetric unit, both molecules are stabilised by characteristic intermolecular C–H···π interactions between hydrogen atoms (H32D, H32E) of the pyridine ring from the Cu1′ complex molecule, and the ring centroids of the quinoline entity from the Cu1 centre (distance of C32D–H32D···centroid (C17–C23) = 2.859 Å, C32E–H32E···centroid (N3–C21) = 2.975 Å, and distance of C32E–H32E···centroid (C17–C23) = 3.467 Å).

The resulting network is reinforced by intermolecular hydrogen bonding interactions where water and acetone molecules are involved (O7–H7B···O5 = 2.020 Å, bond angle = 146.27°; O7–H7A···O36 = 2.236 Å, bond angle = 135.45°).

The solid-state structure of **4** is depicted in Fig. S41.† Due to the low quality of the structure, structural features are not described in detail. However, these data provide the required information about the nature of the molecule in the crystal.

The crystal structure of **6**·$CHCl_3$·0.13H_2O (Fig. 6) is less distorted from the tetrahedral coordination geometry, when compared with [Cu(pqcame)$_2$][PF_6],[27] due to the insertion of the methyl group (C6′). The dihedral angle of 80.82° between the least-squares planes of the two five-membered chelate rings is similar to that of complex **2** and compares well with those reported in the literature for other copper(I) complexes.[16] Typical intermolecular π–π stacking, C–H···π and C–H···O contacts, in the crystal packing of **6**·$CHCl_3$·0.13H_2O, are shown in Fig. S42.†

Complex 2{**7**·C_5H_{12}}·$CHCl_3$ (Fig. 7) crystallizes in the monoclinic space group *C*2/*c*, with two independent molecules (Cu and Cu′) which display significant distortion from that of an ideal tetrahedron. In contrast to complex **6**·$CHCl_3$·0.13H_2O with a methyl at the 6′, the copper(I) complex cation in **7** posses a more flattened structure, as the angles between the least-squares planes containing Cu or Cu′ and each of the chelated rings are 60.35° and 61.01° respectively. The two ligands around the copper centre are not planar and the angles between the planes defined by the pyridine and quinoline entities range from 25.27° to 32.45°. The crystal packing is such that a pair of molecules is stabilised by an intermolecular π–π stacking interaction between the centroids of the N3-containing rings of adjacent quinoline moieties, at a separation of 3.827 Å (Fig. S43†), and non-classical C–H···π contacts (distance of (C27–H27C)···centroid (C18′–23′) = 3.454 Å).[35] Finally, the crystal network is reinforced by non-classical intermolecular hydrogen bonding interactions (C17′–H17′···O4′ = 2.535 Å).[43]

The solid-state structure of **8** (Fig. 8) reveals a distorted tetrahedral coordination geometry, as reported previously for the similar complexes **6** and **7**. The angle between the least-squares planes including a copper(I) centre and each of the **8,6′-Me$_2$pqcam**e bidentate ligands is 68.22°, indicative of a less flattened structure compared with that of **7**. Due to the addition of methyl groups at the 8,6′-positions of the ligand periphery, the quinoline and pyridine moieties of each ligand are not coplanar. Deviation from planarity becomes evident from the angles of 20.95° (between the planes of the rings including N1/N2) and 23.43° (for N3/N4) respectively. The crystal packing of **8** involves typical C–H···π interactions. Thus, the hydrogen atom H30A of the methyl ester group displays a characteristic contact with the centroid of the adjacent benzo ring of quinoline (distance of (C30–H30A)···centroid(C6) = 2.891 Å). Also the distance of (C36–H36C)···centroid(C35–N4) = 3.326 Å, describing the interaction of H36C from a methyl group with the centroid of the pyridine moiety of an adjacent molecule. Notably, a Cambridge Structural Database search revealed that there are very few reports related to copper(I) complexes comprising these ligands.

Electronic spectra

The solution absorption spectra of the homoleptic copper(I) complexes **1–4** are shown in Fig. 9, while those of **5–8** are included in Fig. S44.† All compounds show a main and broad MLCT absorption band centered between 506 nm and 532 nm, while the bands in the region of 333–339 nm are typical of ligand-centered π–π* transitions.

Ongoing from **1** to **2** a small red shift is observed for the main MLCT band from 527 nm (**1**) to 530 nm (**2**), with ε values at approximately 6600 $dm^3\ mol^{-1}\ cm^{-1}$, significantly higher than those of other similar copper(I) diimine complexes.[42] For complexes **3** and **4**, the λ_{max} of the MLCT band blue-shifts to 519 nm and 506 nm respectively, indicating an increase of the

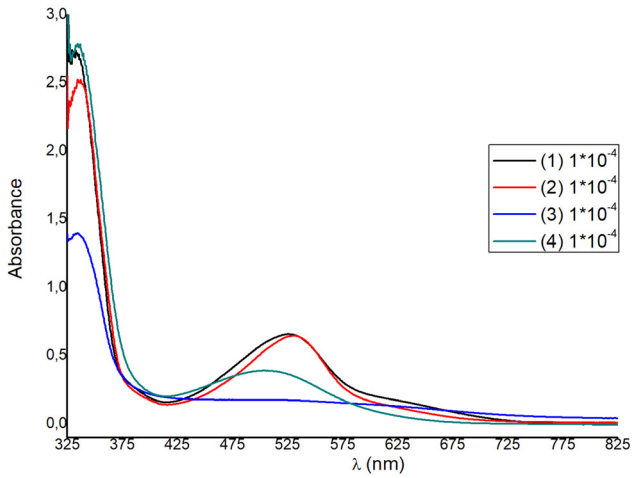

Fig. 9 Absorption spectra of compounds **1–4** in Me_2CO at 298 K.

ΔE band gap. Blue-shifting is accompanied by an approximate four- and two-fold decrease of the extinction coefficient respectively. Within the homoleptic complexes **1–4**, ε values range from 1800 to 6600 $dm^3\ mol^{-1}\ cm^{-1}$ ($\varepsilon_3 < \varepsilon_4 < \varepsilon_1 \approx \varepsilon_2$), while ongoing to the methyl ester analogues **6–8**, the extinction coefficient increases significantly, reaching a value of ~10 000 $dm^3\ mol^{-1}\ cm^{-1}$, for **6**. This is in accord to the ε values reported for $[Cu(pqcame)_2][PF_6]$[27] and other similar complexes in the literature.[44,45]

For DSSC application, dyes **1** and **2** are superior to **3** and **4**, as the spectral window covered by the MLCT absorption band is broader and the extinction coefficients are much higher. For each complex a second, broad shoulder-like, MLCT band is observed around 630 nm, with very low ε values. This is a typical feature reported in the absorption spectra of copper(I) phenanthroline complexes, where generally three bands are observed, which are abbreviated as band I, band II, and band III.[15,44,45] Taking this nomenclature into consideration, we may propose that the broad MLCT band can be attributed to band II, alongside band III, which is typically hidden within band II. The lowest energy MLCT broad band above 600 nm can be potentially attributed to band I, which is indicative of a distorted tetrahedral geometry. This further corroborates with the structural features obtained from the X-ray crystal structure analysis of the compounds studied, indicating a strong distortion from that of the ideal tetrahedral geometry (*vide infra* in Fig. 4–6). In addition, very recent reports further suggest that the highest energy MLCT band (band II) is attributed to an $S_0 \rightarrow S_2$ transition (Franck–Condon level), while band I is attributed to an $S_0 \rightarrow S_1$ charge transfer.[45,46] In particular, the energy and the intensity of the $S_0 \rightarrow S_1$ and $S_0 \rightarrow S_2$ transitions can shift according to geometrical changes, owing to the steric hindrance of the ligands used. Accordingly, $S_0 \rightarrow S_2$ energy shifting may be attributed to a change of the Cu–N bond lengths, while the $S_0 \rightarrow S_1$ transition receives lower values for D_{2d} symmetric compounds.[45,46]

Based on the poor optical characteristics derived from the solution absorption spectrum of **3**, no further studies were undertaken with this complex. We emphasized dyes **1**, **2** with carboxylic acid anchoring ligands and **6** and [Cu(pqcame$_2$][PF$_6$] (**A**) that bear a methyl ester moiety. Sample solutions and dyed films are displayed in Fig. S45.† From visual inspection it becomes evident that **1** and **2** adsorb strongly on the titania surface, but **6** and (**A**) rather slightly. Interestingly, complex **6** incorporating the ester **6′-Mepqcame** gave better dye-modified surfaces compared with that of (**A**), which bears the less sterically demanding **pqcame** ligand.

From the solid-state absorption spectra presented in Fig. 10, it is easily seen that the absorption intensity of the electrode with dye **2** is higher than that of **1**, indicating that **2** is more efficiently adsorbed on the TiO_2 surface. Upon grafting of both dyes onto the titania surface the absorption maxima are blue shifted (22 nm for **1** and 16 nm for **2**) compared with the data obtained in solution. This is an indirect proof of chemisorption of the dyes and may be attributed to deprotonation of the carboxylic acid functionalities, which shifts the orbitals of the anchoring ligand.[26,47] Grafting of **6** onto TiO_2 film is less efficient (Fig. S46†).

Electrochemical studies

The electrochemical characteristics of dyes **1**, **2** and **4** were measured by means of cyclic voltammetry under argon (Fig. S47†), and the relative data are summarized in Table 1.

Cyclic voltammograms were recorded in Me_2CO due to the high solubility and chemical stability of the complexes in this solvent. It was not possible to measure complex **3** in this solvent within the time scale of the measurement, due to partial decomposition. The relevant methyl ester analogues **6–8** were not measured since they chemisorb slightly on the titania surface, while **2** and **4** exhibit a copper-centered oxidation. The oxidation potential for **2** (+0.43 V) is within the range reported for copper(I)-bipyridyl complexes,[18] while the peak separation of 224 mV implies slow electron transfer kine-

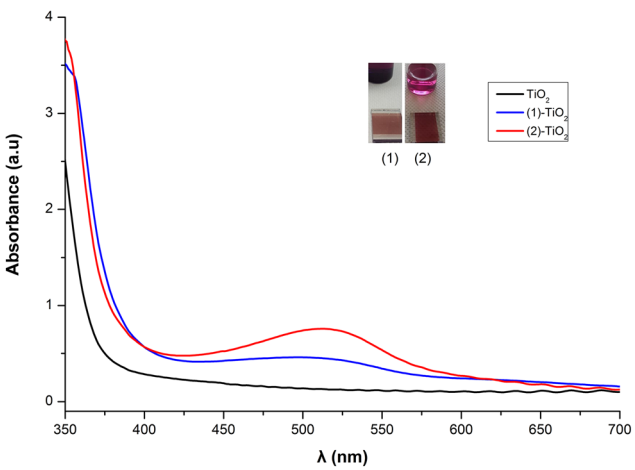

Fig. 10 Dyes **1** and **2** adsorbed on TiO_2.

Table 1 Cyclic voltammetric data for complexes (**1**), (**2**) and (**4**) (potential values reported against the Fc/Fc^+ redox couple); Me_2CO solutions (3 mM) with $[^nBu_4N][PF_6]$ (1 M) as the supporting electrolyte; a scan rate: 0.1 V s^{-1}

Complex	E_{pa} (mV)	E_{pc} (mV)	$E_{1/2}$/V ($\Delta E = E_{pc} - E_{pa}$/mV)
(**1**)	—	—	—
(**2**)	+155	−69	+0.43 (224)
(**4**)	+209	[a]	—

[a] No reduction process observed within the solvent accessible window.

tics. In accord with the literature reports, chemical irreversibility of the redox process is also observed for both complexes (**2** and **4**).[48] In short, the electrochemical behavior of complexes **1**, **2** and **4** follows the expected trend, with complex **2**, containing a methyl substituent at the 6′ position of quinoline, being electrochemically the most stable.[16,49]

The electrochemical characteristics of dye **2** absorbed onto TiO_2 were also measured by means of cyclic voltammetry. A three-electrode, one-compartment electrochemical cell was used for the cyclic voltammetry (CV) measurements with a supporting electrolyte of 0.1 M $[^nBu_4N][PF_6]$ in acetonitrile (MeCN). Metrohm platinum wire was used as the counterelectrode, Ag/AgCl (3 M KCl) as the reference electrode and sensitized TiO_2 films as the working electrodes.

Potentials referred are quoted *versus* Ag/AgCl or +0.77 V *vs.* the standard hydrogen electrode (SHE), where the potential Ag/AgCl (3 M KCl) is +0.21 V. The applied scan rate was 20 mV s^{-1}.

The cyclic voltammogram presented in Fig. 11 displays a characteristic oxidation and reduction wave (E_{pa} = +0.64 V, E_{pc} = +0.47 V) which is attributed to the Cu(I)/Cu(II) system. The peak separation of ~175 mV showed quite slow electron transfer kinetics, so the electrochemical behavior is described as quasi-reversible.[18,50] The half wave potential, $E_{1/2}$, deduced from the cyclic voltammogram curve, determines the highest occupied molecular orbital (HOMO) level of the dye. Thus, the $E_{1/2}$ for the **2** complex is +0.56 V *vs.* Ag/AgCl or +0.77 V *vs.* a standard hydrogen electrode (SHE). This value is sufficiently positive compared with the I^-/I_3^- redox potential (+0.33 V *vs.* SHE), suggesting efficient dye regeneration[51] (*vide infra* in the DSSC evaluation).

The lowest unoccupied molecular orbital (LUMO) level of the dye was estimated from the HOMO level and the excitation energy of the dye adsorbed on TiO_2. The latter was determined from the difference $E_{ox} - E_g$, where E_{ox} stands for the redox potential of the Cu(I)/Cu(II) redox couple and E_g is the absorption threshold of the low-energy tail of the TiO_2/dye absorption spectrum (Fig. S48†), which in the case of **2** is at 2.03 eV (612 nm).[52,53] The LUMO level of **2**, calculated at −1.26 V *vs.* NHE, is sufficiently negative compared with the conduction band (CB) edge of TiO_2 (−0.5 V *vs.* SHE),[54] implying efficient electron injection into the CB of titania.

Based on cyclic voltammetry and UV-vis data, the energy diagram of the interface including the HOMO and LUMO energy levels of dye **2** has been estimated and is depicted in Fig. 12. This would enable us to justify the photovoltaic performance of this complex.

FT-IR and Raman spectroscopic data of the sensitized films

FT-IR spectroscopic data. Sensitization of the titania photoelectrodes by the copper(I) complexes becomes evident by FT-IR spectroscopy (Fig. S49†). In a typical experiment, dried TiO_2 (Degussa P-25, 50 mg) was added into acetone solutions of compounds **1**, **2** and **4** (8×10^{-4}–1×10^{-3} M), and the resulting solutions remained in the dark for two days. After fil-

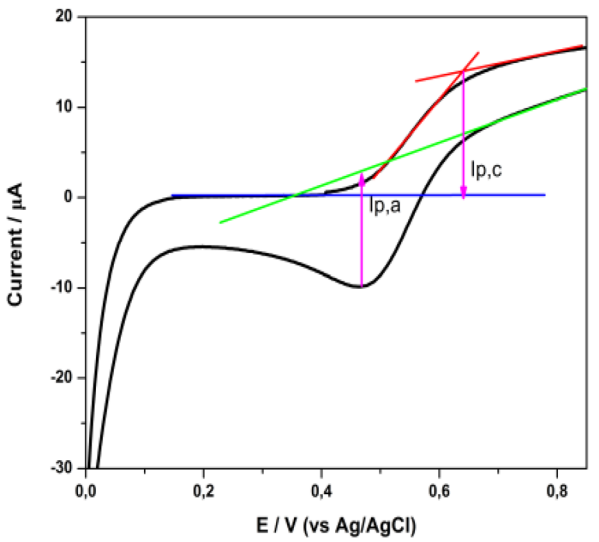

Fig. 11 Cyclic voltammogram of a **2** sensitized titania film, in a three-electrode electrochemical cell.

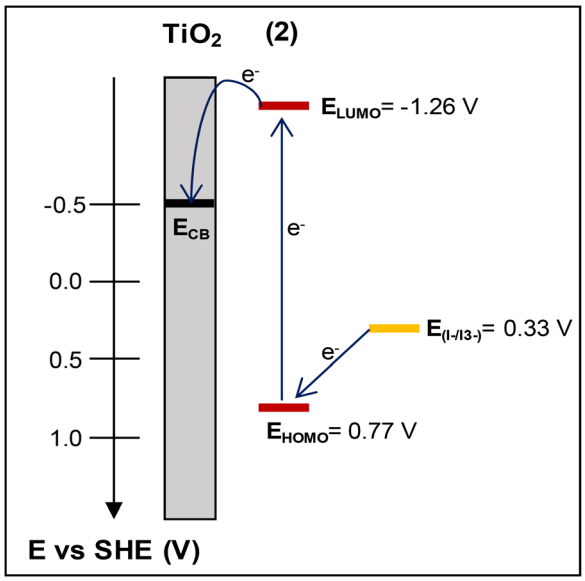

Fig. 12 The energy diagram of the photoelectrode electrolyte interface depicting the HOMO–LUMO energy levels of dye (**2**) *vs.* the conduction band (CB) level of TiO_2 and the redox potential of I^-/I_3^-.

tration, the colored solids were washed successively with acetone and diethyl ether and dried at 40 °C for 48 h. The obtained powders were dispersed in KBr following a well-defined protocol.[55]

The corresponding FT-IR spectra of the dye-sensitized titania nano-powdered films are dominated by the anatase TiO_2 bands, while the dye contribution is relatively poor (weak intensity bands). The broad band centered at ~3500 cm^{-1} corresponds to the characteristic O–H stretching vibration produced by the hydroxyl groups and chemisorbed water on the titania film.[56] The rather sharp band located in the region of 1635–1620 cm^{-1} is due to the bending modes of water (H–O–H) that is overlapped with the Ti–O stretching vibration mode.[52,53] The C═O shift (~1725 cm^{-1} (**1**), 1725 cm^{-1} (**2**), 1727 cm^{-1} (**4**)) was attributed to chemisorption of the dyes onto the titania surface, *via* ester-type bonding.[55] The TiO_2 nanoparticles treated with the new dyes display a number of weak but characteristic IR bands in the typical region of 1565–1300 cm^{-1} that correspond to the pyridine ring modes. This further suggests efficient dye grafting on the titania surface. The absorption band at the lowest part of the spectrum ~700–450 cm^{-1} is related to the Ti–O vibration.[55]

Micro-Raman spectroscopic data. Resonance Raman spectroscopy is an excellent tool to provide us with the required information about the chemisorption of molecular dyes onto the titania surface.[26]

In this respect adsorption of dye **2**, the most prominent for DSSCs, onto the titania film becomes apparent by comparing the micro-Raman spectra of **2** in a powder form and that chemisorbed onto the titania film (Fig. S50†).

The two bands at the lower frequency region (638 cm^{-1} and 143 cm^{-1}) of the spectrum are related to stretching vibrations of the semiconductor. Among them, the most intense band (143 cm^{-1}) is attributed to O–Ti–O vibrations (E_{1g}).[57] Representative fingerprint bands of dye **2** are shown in the 1600–1300 cm^{-1} range: a strong band at 1443 cm^{-1} for C–H bending and the ν(C═N) and ν(C═C) pyridine modes at 1473, 1512, 1550 and 1551 cm^{-1}. The strong band located at 1365 cm^{-1} is attributed to a combination of the in-plane C–H stretching vibrations and the C═C stretching vibrations of the aromatic carbons.[25,57] These bands are also observed in the spectrum of **2** in the powder form.

In comparison with the bare complex (powder form), slight differences either in the peak position or width were observed, implying weak electronic coupling of complex **2** onto the semiconductor surface. This could be attributed to the single carboxylic acid group present in this molecular dye.[26,47]

Photovoltaic performance of the dyes in DSSCs

The photovoltaic performance of nanocrystalline TiO_2 solar cells sensitized by dyes **1** and **2** containing carboxylic acid functionalities, and that of the methyl ester analogues **6** and (**A**), has been evaluated under the standard AM 1.5 irradiation conditions.[26,48] The performance of the homoleptic copper(I) dye **5** that served as a reference herein[12] has been also reported by other research groups.[37,39] For sensitization, the working electrodes were immersed in a solution of the dye and left undisturbed overnight (see the experimental part).

The influence of the architecture of the modified electrodes (photoanodes) on the resulting performance of the photovoltaic device, assembled with the most promising dyes, was investigated. Typical photocurrent density–photovoltage *J–V* curves of **1**, **2**, **A** and **6**-sensitized solar cells are depicted in Fig. 13. The lower case letters (a–d) highlight the different architectures of the semiconductor material of the anode, dyed with **1** and **2**, as reported in Table 2 (*vide infra*). A comparison of the best performing film (**2d** in Table 2) with the **5** cell reference is shown in Fig. S51.†

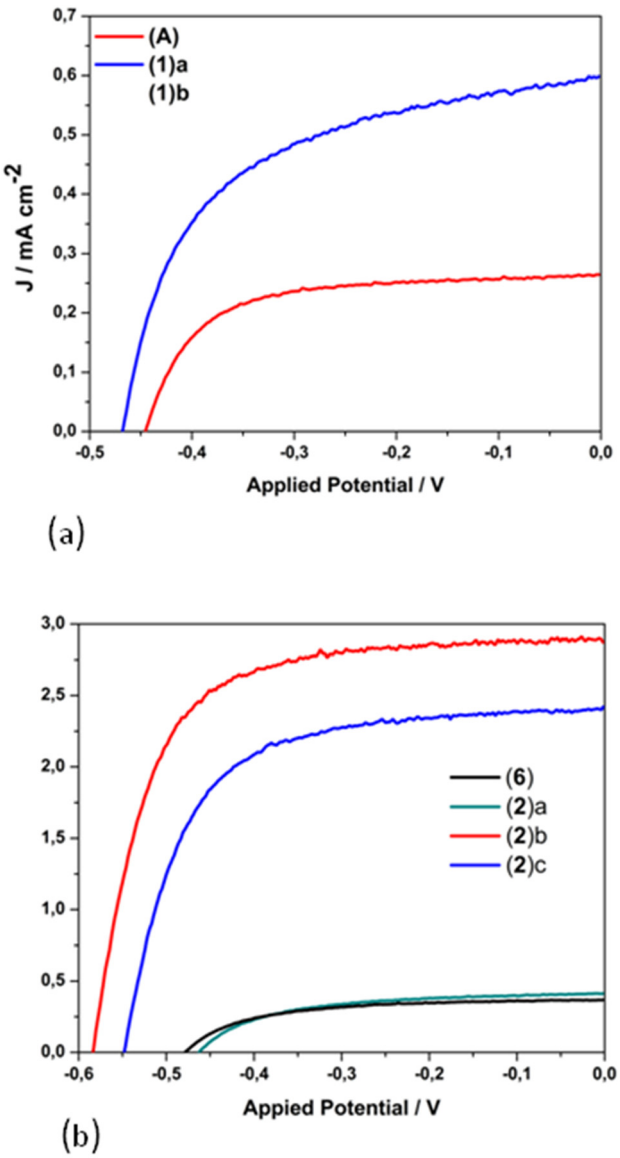

Fig. 13 *J–V* curves for the copper(I)-based dyes **1**, [Cu(pqcame$_2$][PF_6] (**A**) (a); **2** and **6** (b). Lower case letters highlight the different architecture of the semiconductor material of the anode, dyed with **1** and **2**, as reported in Table 2.

Table 2 Photovoltaic parameters (J_{sc}, V_{oc}, FF, and η) of DSSCs incorporating the dyes **1**, **2**, **A**, **5** and **6** measured under the same experimental conditions

Anode-dye (entry)	Film (+post-treatment)	J_{sc}/mA cm^{-2}	V_{oc}/mV	FF	η/%
1(a)	NRT	0.26	446	0.66	0.08
1(b)	NRAO–WER4	0.60	470	0.55	0.15
2(a)	NRT	0.41	465	0.56	0.11
2(b)	NRAO–WER4	2.87	585	0.68	1.15
2(c)	DSL–NRAO–WER4	2.42	549	0.64	0.85
2(d)	CL–NRAO–WER4	2.94	591	0.69	1.20
A	NRAO–WER4	0.28	443	0.43	0.05
5	CL–NRAO–WER4	2.90	576	0.63	1.05
6	NRAO–WER4	0.37	480	0.57	0.10

NRT = transparent titania paste, NRAO = active opaque titania paste, WER4 = scattering layer, CL = compact layer, DSL = transparent titania paste (3 μm layer).

The corresponding electrical parameters or cell characteristics (short-circuit current density (J_{sc}), open-circuit voltage (V_{oc}); fill factor (FF) and power conversion efficiency (η)) of all the fabricated DSSCs are reported in Table 2 (the mean value of three essays). From this Table it is clearly seen that photoanodes consisting of only one transparent titania layer (NRT, entry a), dyed with **1** and **2**, display a very poor performance of approximately 0.1% (**1**(a), η = 0.08% and **2**(a), η = 0.11%). On the other hand, the combination of an active layer (NRAO) and a scattering layer (WER4) leads to a substantial tenfold increase in the power conversion efficiency of dye **2** (η = 1.15%, entry **2(b)**), while that of **1** is doubled (η = 0.15%, entry **1(b)**).

This is mainly attributed to the marginal increase of the J_{sc} (2.87 mA cm^{-2}) and a rise of the open circuit potential by 115 mV. Apparently, the existence of the scattering layer plays a crucial role (increase of the optical path length) for the increased performance of photovoltaic devices sensitized with dye **2**.[58] Interestingly, a decrease in the performance of a device assembled with three layers of titania (entry **2c**) was observed (absence of a compact layer), as the J_{sc} and V_{oc} values drop to 2.42 mA cm^{-2} and 549 mV respectively. However, a further improvement in the performance of the cell device was obtained upon $TiCl_4$ pre-treatment of the anode.[59] This procedure proved beneficial for the optimization of the device, as indicated by a slight increase of the short circuit current and a slight enhancement of the V_{oc}. As a result, the most efficient cell displayed J_{sc}, V_{oc} and power energy-conversion efficiency (PCE-η) values of 2.94 mA cm^{-2}, 591 mV and 1.20% respectively (entry **2(d)**). To this end, the **2**-based cell device is the most efficient, with a relative power conversion efficiency exceeding by 13% that of the reference **5**, measured under the same experimental conditions (entry **5**). Overall, the efficiency of **2** shows a gain in terms of the V_{oc} value.

To test the viability of copper(I) complexes **A** and **6** with methyl ester functionalities in DSSCs and improve the initially poor photovoltaic characteristics reported above, we decided to use the protocol of He *et al.* for a Zn(II) sensitizer[60] and that of Kee and coworkers for homoleptic copper(I) dyes.[49] Accordingly, and prior to dye dipping, the photoanode was pre-treated with *t*BuOK/THF as described in eqn (1).

$$\text{–Ti-OH} + t\text{BuOK} \rightarrow \text{–Ti-OK} + t\text{BuOH} \quad (1a)$$

$$\text{–Ti-OK} + \text{Dye-COOR} \rightarrow \text{–Ti-OOC-Dye} + \text{ROK (R = Me)} \quad (1b)$$

However, the application of the protocol led to a degradation of the surface characteristics (Fig. S52†) with a concomitant decrease of the performances (<0.01%), to significantly lower than the performances reported for non-pre-treated photoelectrodes (Table 2). In any case, the photovoltaic performances of **A** (0.05%) and **6** (0.10%) were significantly higher than those reported for other copper(I) complexes incorporating methyl ester functionalities.[49]

To this end, these results are in favor of a great potency of the new copper(I) molecular compounds, as compared with ruthenium(II) congeners that display similar photovoltaic data, in terms of the significantly low cost and higher availability of the Earth-abundant copper-based precursors. Besides their potency for applications in window-glass building facades, investigation of the photosensitization process may be facilitated by their usage as copper redox mediators.[61,62]

Experimental

Materials and methods

All manipulations concerning the synthesis of the copper(I) complexes were carried out under argon using standard Schlenk techniques, while the synthesis of the ligands was performed under aerobic conditions. The solvents were dried by standard methods (MeCN and CH_2Cl_2 over P_2O_5, diethyl ether (Et_2O) over Na wire, Me_2CO over K_2CO_3) and distilled under argon. DMSO (Me_2SO) was dried over freshly activated molecular sieves of 4 Å, and methanol over molecular sieves of 3 Å. The distilled solvents were stored over molecular sieves under an argon atmosphere. All solvents were thoroughly degassed by three freeze–pump–thaw cycles prior to use.

The copper(I) precursor $[Cu(MeCN)_4][PF_6]$ was synthesised according to the literature reports.[63] The **pqca** ligand was prepared by a slight modification of the reported procedure[64] while its methyl ester analogue (**pqcame**) was prepared according to the method reported in the literature.[27] 7-Methylisatin,[65,66] 6-methylpicolinic acid,[67] ethyl-6-methylpicolinate,[68] 2-acetyl-6-methyl-pyridine,[69] and 6,6′-dimethyl-2,2′-bipyridine-4,4′-dicarboxylic acid (dmdcbpy),[12,70] used for the synthesis of the organic ligands, were prepared according to the literature methods and their purity was tested by FT-IR, ^{1}H NMR and melting point measurements.

Elemental analyses were obtained from the Microanalysis Center of the Institut für Anorganische Chemie Universität Bonn. Infrared spectra were measured on a Shimadzu IRAffinity-1 spectrometer, as potassium bromide pellets in the spectral range of 4000–400 cm^{-1}. ^{1}H and ^{13}C{^{1}H} NMR spectra were recorded at 298 K on a Bruker Avance DRX 500 MHz, a Bruker Prodigy 500 MHz and a Bruker Avance Neo 400 MHz

spectrometer in $CDCl_3$, Me_2CO-d_6 and DMSO-d_6. The ^1H and $^{13}C\{^1H\}$ NMR spectra were calibrated against the internal residual proton and natural abundance ^{13}C resonances of the deuterated solvent. *J* values are given in Hz. Spectra were assigned using the ^1H–^1H COSY, ^1H–^{13}C HSQC and ^1H–^{13}C HMBC methods. Melting or decomposition points were determined using a Sanyo Gallenkamp variable heater apparatus and are uncorrected. The samples were heated slowly until the compounds melted or decomposed. Micro-Raman spectra were measured in the backscattering configuration using a Renishaw inVia Reflex system equipped with an Ar laser emitting at 514.4 nm. The scattered light is filtered by a dielectric edge Rayleigh rejection filter with cutoff at 100 cm^{-1} and analyzed with an 1800 lines per mm diffraction grating. Laser power was set to 0.1% to avoid dye degradation. Absorption spectra were recorded with a Cary 3E UV-vis spectrometer in acetone or chloroform solution. A three-electrode, one-compartment electrochemical cell was used for the cyclic voltammetry (CV) measurements with a supporting electrolyte of 0.1 M tetrabutylammonium hexafluoridophosphate [TBA][PF_6] in acetonitrile. Metrohm platinum wire was used as a counter-electrode, Ag/AgCl (3 M KCl) as the reference electrode and sensitised TiO_2 films as the working electrodes. Potentials referred to are quoted *versus* the standard hydrogen electrode (SHE), where Ag/AgCl (3 M KCl) is +0.21 V.

Synthesis of organic precursors with COOH groups

pqca. This compound was prepared according to the published procedure.[29] However, the recrystallization reported in the final step is not necessary. **Pqca** can be obtained in high purity after initial washing with water and ethanol and subsequent rinsing with acetone and diethyl ether. The purity of the bulk substance was checked by ^1H NMR spectroscopy.

6′-Mepqca. In a round bottom flask, isatin (1.105 g, 0.0075 mol) was dissolved in 6 mL of 33% (w/w) aqueous KOH solution. To the clear orange solution, 2-acetyl-6-methylpyridine (1 g, 0.0074 mol) in ethanol (10 mL) was added, and the resulting mixture was heated in a reflux process for 18 h. After this time, excess ethanol was rotary-evaporated, and the resulting slurry was cooled and filtered. The obtained beige solid was dried for 1 h and then washed successively with acetone (2 × 5 mL) and diethyl ether (3 × 7 mL) and vacuum-dried overnight. Then it was dissolved in the minimum amount of slightly warm water and the solution was acidified with 2 M $HCl_{(aq)}$, until pH = 4.3 was obtained. The solvent was evaporated under mild heating until precipitation occurred and the mixture was cooled in an ice/water bath to afford **6′-Mepqca**, which was washed with cold water (2 × 3 mL), cold acetone (3 × 5 mL) and diethyl ether (3 × 10 mL) and dried under vacuum for 16 h and then in an oven at 80 °C overnight. Yield: (1.39 g, 50%). Decomp. >218 °C. Found: C, 69.5; H, 4.6; N, 10.05. $C_{16}H_{12}N_2O_2{\cdot}0.7H_2O$ requires C, 69.4; H, 4.9; N, 10.1%. IR (KBr, ν_{max}/cm^{-1}): 3055 (m, ν(C–H)$_{arom}$), 2929 (m, ν_{as}(C–H)$_{aliph}$), 2865 (w, ν_s(C–H)$_{aliph}$), 1694 (vs, ν_{as}(C═O)), 1588 (s, ν(C═C)), 1554 (m, ν(C═C)), 1453 (s, ν(C═N)), 1286 (s), 1261 (s), 901 (m, br, δ(O–H)), 795 (s, γ(C–H)$_{out\text{-}of\text{-}plane}$), 773 (s, γ(C–H)$_{out\text{-}of\text{-}plane}$), 732 (s, γ(C–H)$_{out\text{-}of\text{-}plane}$), 654 (s, γ(C–H)$_{out\text{-}of\text{-}plane}$). ^1H NMR (500 MHz, DMSO-d_6) δH/ppm 14.05 (1H, br s, COOH), 8.99 (1H, s, H3), 8.76 (1H, d, *J* = 10, H9), 8.43 (1H, d, *J* = 10 Hz, H3′), 8.19 (1H, d, *J* = 10, H6), 7.91 (1H, t, *J* = 10, H4′), 7.87 (1H, d, *J* = 10, H7), 7.74 (1H, t, *J* = 10, H8), 7.41 (1H, d, *J* = 10, H5′), 2.63 (3H, s, Me of pyridine ring). $^{13}C\{^1H\}$ NMR δC/ppm (126 MHz, DMSO-d_6) 167.57 (COOH), 157.80 (C6′), 155.27 (C2′), 153.77 (C2), 148.16 (C10), 137.65 (C4′), 137.03 (C4), 130.11 (C7), 129.88 (C6), 128.22 (C8), 125.55 (C9), 124.44 (C5), 124.33 (C5′), 119.22, 118.17 (C3′), 24.19 (Me of pyridine ring); ESI-MS (MeOH, positive mode): *m*/*z* 279.1 $[M + H]^+$ (calc. 279.3).

8-Mepqca. This compound was isolated as a white solid, following the procedure reported for the **6′-Mepqca** diimine analogue, upon treatment of 7-methyl-isatin (1.21 g, 0.0075 mol) and 2-acetylpyridine (0.9 g, 0.0075 mol) in the presence of 33% (w/w) aqueous KOH solution (6 mL) and ethanol (10 mL). Yield: (1.50 g, 73%). Decomp. >295 °C. Found: C, 68.7; H, 4.6; N, 9.9. $C_{16}H_{12}N_2O_2{\cdot}H_2O$ requires C, 68.5; H, 5.0; N, 10.0%. IR (KBr, ν_{max}/cm^{-1}): 3025 (m, ν(C–H)$_{arom}$), 2925 (m, ν_{as}(C–H)$_{aliph}$), 2848 (w, ν_s(C–H)$_{aliph}$), 1690 (vs, ν_{as}(C═O)), 1599 (s, ν(C═C)), 1556 (m, ν(C═C)), 1480 (s, ν(C═N)), 1269 (s, ν_s(C–O), 1244 (s, ν(C–O)), 916 (m, br, ν(O–H)), 794 (s, γ(C–H)$_{out\text{-}of\text{-}plane}$), 772 (s, γ(C–H)$_{out\text{-}of\text{-}plane}$), 740 (s, γ(C–H)$_{out\text{-}of\text{-}plane}$), 716 (s, γ(C–H)$_{out\text{-}of\text{-}plane}$), 648 (s, γ(C–H)$_{out\text{-}of\text{-}plane}$). ^1H NMR (400 MHz, DMSO-d_6) δH/ppm 13.85 (1H, br s, COOH), 8.98 (1H, s, H3), 8.79 (1H, br s, H6′), 8.69 (1H, br s, H3′), 8.58 (1H, br s, H6), 8.07 (1H, br s, H4′), 7.73 (1H, br s, H8), 7.62 (1H, br s, H7), 7.55 (1H, br s, H5′), 2.87 (3H, s, Me of quinoline ring). $^{13}C\{^1H\}$ NMR(100 MHz, DMSO-d_6) δC/ppm 167.80 (COOH), 154.89 (C2), 153.76 (C2′), 149.40 (C6′), 147.02 (C10), 137.90 (C4), 137.55 (C4′), 137.27 (C9), 130.15 (C8), 127.99 (C7), 124.88 (C5′), 124.49 (C5), 123.43 (C6), 121.08 (C3′), 118.61 (C3), 17.98 (Me of quinoline ring).

8,6′-Me_2pqca. As for the previous compounds: 7-methyl-isatin (1.21 g, 0.0075 mol) and 2-acetyl-6-methylpyridine (1 g, 0.0074 mmol) in the presence of 33% (w/w) aqueous KOH solution (6 mL) and ethanol (10 mL). Yield: (1.28 g, 47%). Decomp. >235 °C. Found: C, 72.7; H, 5.15; N, 9.9. $C_{17}H_{14}N_2O_2{\cdot}0.2H_2O$ requires C, 72.4; H, 5.15; N, 9.9%. IR (KBr, ν_{max}/cm^{-1}): 3055 (m, ν(C–H)$_{arom}$), 2919 (m, ν_{as}(C–H)$_{aliph}$), 2840 (w, ν_s(C–H)$_{aliph}$), 1693 (vs, ν_{as}(C═O)), 1591 (s, ν(C═C)), 1561 (m, ν(C═C)), 1457 (s, ν(C═N)), 1284 (s), 1262 (s), 918 (m, br, δ(O–H)), 802 (s, γ(C–H)$_{out\text{-}of\text{-}plane}$), 773 (s, γ(C–H)$_{out\text{-}of\text{-}plane}$), 763 (s, γ(C–H)$_{out\text{-}of\text{-}plane}$), 736 (s, γ(C–H)$_{out\text{-}of\text{-}plane}$). ^1H NMR (400 MHz, DMSO-d_6) δH/ppm 8.94 (1H, s, H3), 8.54 (1H, d, *J* = 8, H6), 8.46 (1H, d, *J* = 8, H3′), 7.91 (1H, t, *J* = 8, H4′), 7.71 (1H, d, *J* = 8, H8), 7.60 (1H, t, *J* = 8, H7), 7.39 (1H, d, *J* = 8, H5′), 2.85 (3H, s, Me of quinoline ring), 2.62 (3H, s, Me of pyridine ring). $^{13}C\{^1H\}$ NMR (100 MHz, DMSO-d_6) δC/ppm 167.80 (COOH), 157.72 (C6′), 154.11 (C2), 153.86 (C2′), 147.00 (C10), 137.65 (C4′), 137.40 (C4), 137.23 (C9), 130.08 (C8), 127.91 (C7), 124.38 (C5), 124.21 (C5′), 123.34 (C6), 118.64 (C3), 118.19 (C3′), 24.20 (Me of pyridine ring), 17.97 (Me of quinoline ring).

General synthetic procedure of the methyl ester analogues

In a round bottom flask, 1 mmol of the **8-Mepqca** (**6′-Mepqca** or **8,6′-Me$_2$pqca**) precursor was dispersed in MeOH (25 mL). To this solution, 1.2 mL of conc. H_2SO_4 was added dropwise, and the slightly yellow solution was refluxed overnight. The organic solvent was evaporated, and the residue was diluted with water (15 mL). The pH of the mixture was adjusted to ~8–9 (30% w/w NaOH(aq)), leading to the precipitation of a white solid, which was filtered, washed with distilled H_2O (2 × 5 mL), and dried *in vacuo* for 24 h. Finally, the solid was dried in a vacuum desiccator under P_2O_5.

6′-Mepqcame. Off-white solid. Yield: (0.25 g, 85%). Decomp. >130 °C. Found: C, 72.5; H, 5.2; N, 9.8. $C_{17}H_{14}N_2O_2{\cdot}0.2H_2O$ requires C, 72.4; H, 5.15; N, 9.9%. IR (KBr, ν_{max}/cm^{-1}): 3008 (m, ν(C–H)$_{arom}$), 2956 (s, ν_{as}(C–H)$_{aliph}$), 2924 (vs, ν_{as}(C–H)$_{aliph}$), 2851 (s, ν_s(C–H)$_{aliph}$), 1723 (vs, ν_{as}(C═O)), 1595 (s, ν(C═C)), 1587 (s, ν(C═C)), 1455 (s, ν(C═N)), 1238 (s), 1220 (s), 1140 (s, ν_{as}(O–CH$_3$)), 797 (vs, γ(C–H)$_{out\text{-}of\text{-}plane}$), 773 (vs, γ(C–H)$_{out\text{-}of\text{-}plane}$), 733 (s, γ(C–H)$_{out\text{-}of\text{-}plane}$). ^{1}H NMR (500 MHz, $CDCl_3$) δH/ppm 9.08 (1H, s, H3), 8.76 (1H, d, J = 10, H9), 8.46 (1H, d, J = 10, H3′), 8.23 (1H, d, J = 10, H6), 7.77 (2H, t, J = 10, H7/H4′), 7.65 (1H, t, J = 10, H8), 7.24 (1H, d, J = 10, H5′), 4.09 (3H, s, COOMe), 2.71 (3H, s, Me of pyridine ring). ^{13}C{^{1}H} NMR (126 MHz, $CDCl_3$) δC/ppm 167.16 (*C*OOMe), 158.25 (C6′), 156.17 (C2′), 155.03 (C2), 148.99 (C10), 137.35 (C4′), 135.82 (C4), 130.51 (C6), 129.87 (C7), 128.29 (C8), 125.67 (C9), 125.12 (C5), 124.10 (C5′), 120.60 (C3), 118.88 (C3′), 52.78 (COOMe), 24.75 (Me of pyridine ring).

8-Mepqcame. Off-white solid. Yield: (0.2 g, 72%). Decomp. >126 °C. Found: C, 72.5; H, 5.1; N, 9.7. $C_{17}H_{14}N_2O_2{\cdot}0.25H_2O$ requires C, 72.2; H, 5.2; N, 9.9%. IR (KBr, ν_{max}/cm^{-1}): 3003 (m, ν(C–H)$_{arom}$), 2955 (s, ν_{as}(C–H)$_{aliph}$), 2917 (vs, ν_{as}(C–H)$_{aliph}$), 2849 (s, ν_s(C–H)$_{aliph}$), 1725 (vs, ν_{as}(C═O)), 1588 (s, ν(C═C)), 1558 (s, ν(C═C)), 1477 (s, ν(C═N)), 1266 (s), 1246 (s), 1105 (s, ν_{as}(O–CH$_3$)), 797 (vs, γ(C–H)$_{out\text{-}of\text{-}plane}$), 770 (vs, γ(C–H)$_{out\text{-}of\text{-}plane}$), 740 (s, γ(C–H)$_{out\text{-}of\text{-}plane}$). ^{1}H NMR (400 MHz, $CDCl_3$) δH/ppm 9.06 (1H, s, H3), 8.75–8.71 (2H, m, H3′/H6′), 8.59 (1H, d, J = 8, H6), 7.87 (1H, br s, H4′), 7.61 (1H, d, J = 8, H8), 7.52 (1H, br s, H7), 7.36 (1H, br s, H5′), 4.05 (3H, s, COOMe), 2.92 (3H, s, Me of quinoline ring). ^{13}C{^{1}H} NMR (100 MHz, $CDCl_3$) δC/ppm 167.24 (*C*OOMe), 156.07 (C2′), 154.17 (C2), 149.26 (C6′), 147.86 (C10), 138.20 (C9), 137.06 (C4′), 136.14 (C4), 130.09 (C8), 128.17 (C7), 125.20 (C5), 124.34 (C5′), 123.48 (C6), 121.78 (C3′), 119.73 (C3), 52.69 (COOMe), 18.53 (Me of quinoline ring).

8,6′-Me$_2$pqcame. Light yellow solid. Yield: (0.23 g, 79%). Decomp. >154 °C. Found: C, 73.6; H, 5.7; N, 9.2. $C_{18}H_{16}N_2O_2{\cdot}0.15H_2O$ requires C, 73.5; H, 5.5; N, 9.5%. IR (KBr, ν_{max}/cm^{-1}): 3009 (m, ν(C–H)$_{arom}$), 2959 (s, ν_{as}(C–H)$_{aliph}$), 2918 (vs, ν_{as}(C–H)$_{aliph}$), 2849 (s, ν_s(C–H)$_{aliph}$), 1721 (vs, ν_{as}(C═O)), 1592 (s, ν(C═C)), 1561 (s, ν(C═C)), 1456 (s, ν(C═N)), 1241 (s), 1222 (s), 1114 (s, ν_{as}(O–CH$_3$)), 806 (s, γ(C–H$_{out\text{-}of\text{-}plane}$)), 772 (vs, γ(C–H$_{out\text{-}of\text{-}plane}$)), 736 (s, γ(C–H$_{out\text{-}of\text{-}plane}$)). ^{1}H NMR (400 MHz, $CDCl_3$) δH/ppm 9.07 (1H, s, H3), 8.56 (1H, d, J = 8, H6), 8.52 (1H, d, J = 8 Hz, H3′), 7.75 (1H, t, J = 8, H4′), 7.61 (1H, d, J = 8, H8), 7.52 (1H, t, J = 8, H7), 7.22 (1H, d, J = 8, H5′), 4.07 (3H, s, COOMe), 2.92 (3H, s, Me of quinoline), 2.69 (s, 3H, Me of pyridine ring). ^{13}C{^{1}H} NMR (100 MHz, $CDCl_3$) δC/ppm 167.46 (*C*OOMe), 158.08 (C6′), 155.45 (C2), 154.58 (C2′), 147.88 (C10), 138.21 (C9), 137.18 (C4′), 136.17 (C4), 129.99 (C8), 127.99 (C7), 125.08 (C5), 123.88 (C5′), 123.46 (C6), 119.83 (C3), 118.77 (C3′), 52.71 (COO*C*H$_3$), 24.76 (Me of pyridine ring), 18.54 (Me of quinoline ring).

Synthesis of copper(I) complexes 1–4

[Cu(pqca)$_2$][PF$_6$]·0.6DMSO (1·0.6DMSO). In a Schlenk tube 120 mg (0.48 mmol) of pqca was dissolved in slightly warm DMSO (10 mL), and 89 mg (0.24 mmol) of [Cu(MeCN)$_4$][PF$_6$] was added in small portions, affording a dark purple solution that was stirred at ambient temperature for 1 h. The volume of the solution was reduced to approximately 1 mL and a mixture of acetone/diethyl ether was added (1/10, v/v) for precipitation of the complex. This procedure was followed four times, affording **1·0.6DMSO** as a black-purple solid that was dried under vacuum at ambient temperature for 10 h. Yield: (0.13 g, 72%). Decomp. >206 °C. Found: C, 50.1; H, 3.4; N, 7.3; S, 2.5. $C_{30}H_{20}CuF_6N_4O_4P{\cdot}0.6DMSO$ requires C, 49.6; H, 3.2; N, 7.4; S, 2.5%. IR (KBr, ν_{max}/cm^{-1}): 3073 (m, ν(C–H)$_{arom}$), 2917 (m, ν_{as}(C–H)$_{aliph}$), 2873 (w, ν_s(C–H)$_{aliph}$), 1718 (s, ν_{as}(C═O)), 1600 (s, ν(C═C)), 1575 (m, ν(C═C)), 1473 (s, ν(C═N)), 1249 (s, ν_s(C–O)), 844 (vs, ν_3(P–F)), 799 (s, γ(C–H)$_{out\text{-}of\text{-}plane}$), 777 (s, γ(C–H)$_{out\text{-}of\text{-}plane}$), 557 (s, ν_4(P–F)). UV-vis (Me_2CO, 1.0 × 10^{-4} mol dm^{-3}): λ_{max}/nm 334 (ε/dm^3 mol^{-1} cm^{-1} 27 200), 527 (6600). ^{1}H NMR (500 MHz, Me_2CO-d_6) δH/ppm 9.20 (1H, br s, H3), 9.05 (1H, br s, H3′), 8.94 (1H, br s, H9), 8.77 (1 H, br s, H6′), 8.38 (1H, br s, H4′), 8.09 (1H, br s, H6), 7.79 (1H, br s, H5′), 7.71 (1H, br s, H8), 7.54 (1H, br s, H7), 2.67 (3.6H, s, Me of DMSO). ^{13}C{^{1}H} NMR (126 MHz, Me_2CO-d_6) δC/ppm 154.33 (COOH), 153.33 (C2), 152.78 (C2′), 150.33 (C6′), 147.33 (C10), 140.44 (C4), 139.72 (C4′), 132.18 (C7), 130.62 (C8), 129.93 (C6), 128.56 (C5′), 126.96 (C9), 124.63 (C3′), 124.39 (C5), 121.53 (C3), 40.66 (Me of DMSO). ESI-MS (MeOH, positive mode): m/z 563.08 [M–PF_6]$^+$ (calc. 563.08, base peak).

[Cu(6′-Mepqca)$_2$][PF$_6$]·0.9DMSO (2·0.9DMSO). In a Schlenk tube 78 mg (0.295 mmol) of 6′-Mepqca was dissolved in slightly warm DMSO (3 mL), giving a colorless solution. [Cu(MeCN)$_4$][PF$_6$] (55 mg, 0.147 mmol) was then added and the resulting dark purple solution was stirred at ambient temperature for 1 h. The volume of the solution was reduced almost to dryness and a mixture of acetone/diethyl ether was added (1/20, v/v) for solidification of the residue. After filtration, the dark purple solid was washed twice with a mixture of acetone/diethyl ether (1/30, v/v) and dried under vacuum at ambient temperature for 10 h. Yield: (0.095 g, 80%). Decomp. >182 °C. Found: C, 50.2; H, 3.8; N, 6.9; S, 3.6. $C_{32}H_{24}CuF_6N_4O_4P{\cdot}0.9DMSO$ requires C, 50.3; H, 3.7; N, 6.9; S, 3.6%. IR (KBr, ν_{max}/cm^{-1}): 3073 (m, ν(C–H)$_{arom}$), 2917 (m, ν_{as}(C–H)$_{aliph}$), 2873 (w, ν_s(C–H)$_{aliph}$), 1718 (s, ν_{as}(C═O)), 1600 (s, ν(C═C)), 1575 (m, ν(C═C)), 1473 (s, ν(C═N)), 1249 (s, ν_s(C–O)), 844 (vs, ν_3(P–F)), 799 (s, γ(C–H)$_{out\text{-}of\text{-}plane}$), 777 (s, γ(C–H)$_{out\text{-}of\text{-}plane}$), 557 (s, ν_4(P–F)). UV-vis (Me_2CO, 1.0 × 10^{-4} mol

dm^{-3}): λ_{max}/nm 334 (ε/dm^3 mol^{-1} cm^{-1} 25 300), 530 (6500). ^{1}H NMR (500 MHz, Me_2CO-d_6) δH/ppm 9.22 (1H, s, H3), 8.95 (1H, d, J = 10, H3′), 8.90 (1H, d, J = 10, H9), 8.32 (1H, t, J = 10, H4′), 8.06 (1H, d, J = 10, H6), 7.77 (1H, d, J = 10, H5′), 7.73 (1H, t, J = 10, H8), 7.55 (2H, t, J = 10, H7), 2.62 (5.4H s, Me of DMSO), 2.26 (3H, s, Me of pyridine ring). ^{13}C{^{1}H} NMR (126 MHz, Me_2CO-d_6) δC/ppm 167.20 (COOH), 159.16 (C6′), 153.56 (C2), 152.12 (C2′), 147.14 (C10), 140.06 (C4′), 139.10 (C4), 132.43 (C7), 130.72 (C8), 129.54 (C6), 128.27 (C5′), 127.54 (C5), 127.08 (C9), 122.26 (C3′), 121.71 (C3), 41.14 (Me of DMSO), 25.18 (CH_3). ESI-MS (MeOH, positive mode): m/z 592.10 [M + H–PF_6]$^+$ (calc. 591.10, [M–PF_6]$^+$, base peak).

[Cu(8-Mepqca)$_2$][PF$_6$] (3). In a Schlenk flask, 8-Mepqca (50 mg, 0.19 mmol) was suspended in Me_2CO (10 mL). Subsequently, 35 mg (0.094 mmol) of [Cu(MeCN)$_4$][PF$_6$] was added and the dark purple solution was stirred for 1 h at 25 °C. After this time, the mixture was filtered, and the volume of the filtrate was reduced under vacuum almost to dryness. The residue was treated with diethyl ether (2 × 10 mL) and the resulting black–purple solid was dried under vacuum at 50 °C for 24 h. Yield: (0.05 g, 75%). Decomp. >210 (°C.). Found: C, 46.1; H, 4.3; N, 6.6. $C_{32}H_{24}CuF_6N_4O_4P{\cdot}5.5H_2O$ requires C, 46.0; H, 4.2; N, 6.7%. IR (KBr, ν_{max}/cm^{-1}): 3096 (m, ν(C–H)$_{arom}$), 2926 (m, ν_{as}(C–H)$_{aliph}$), 2860 (w, ν_s(C–H)$_{aliph}$), 1711 (s, ν_{as}(C=O)), 1599 (s, ν(C=C)), 1550 (m, ν(C=C)), 1479 (s, ν(C=N)), 1260 (s, ν_s(C–O)), 842 (vs, ν_3(P–F)), 771 (s, γ(C–H)$_{out\text{-}of\text{-}plane}$), 742 (m, γ(C–H)$_{out\text{-}of\text{-}plane}$), 558 (s, ν_4(P–F). UV-vis (Me_2CO,1.0 × 10^{-4} mol dm^{-3}): λ_{max}/nm 335 (ε/dm^3 mol^{-1} cm^{-1} 14 000), 519 (1800). ^{1}H NMR (400 MHz, Me_2CO-d_6) δH/ppm 8.94–8.74 (3H, m, H-pqca), 8.41 (2H, m, H-pqca), 7.68 (3H, m, H-pqca), 2.83 (3H, s, Me of quinoline).

[Cu(8,6′-Me$_2$pqca)$_2$][PF$_6$] (4). In a Schlenk tube, 102 mg (0.36 mmol) of 8,6′-Me_2pqca was dissolved in slightly warm Me_2CO (15 mL), affording a clear slight yellow solution. 68 mg (0.18 mmol) of [Cu(MeCN)$_4$][PF$_6$] was then added to the solution of the ligand, affording a deep red solution that was stirred at room temperature for 1 h. The solvent was evaporated almost to dryness, the residue was treated successively with diethyl ether (3 × 7 mL) and the resulting red solid was dried under vacuum at 50 °C for 24 h. Yield: (0.10 g, 92%). Decomp. >195 °C. Found: C, 52.9; H, 4.1; N, 6.9. $C_{34}H_{28}CuF_6N_4O_4P{\cdot}0.5H_2O$ requires C, 52.8; H, 3.8; N, 7.2%. IR (KBr, ν_{max}/cm^{-1}): 3090 (m, ν(C–H)$_{arom}$), 2923 (m, ν_{as}(C–H)$_{aliph}$), 2854 (w, ν_s(C–H)$_{aliph}$), 1712 (s, ν_{as}(C=O)), 1602 (s, ν(C=C)), 1572 (m, ν(C=C)), 1473 (s, ν(C=N)), 1262 (s, ν_s(C–O)), 843 (vs, ν_3(P–F)), 773 (s, γ(C–H)$_{out\text{-}of\text{-}plane}$), 740 (m, γ(C–H)$_{out\text{-}of\text{-}plane}$), 557 (s, ν_4(P–F)). UV-vis (Me_2CO, 1.0 × 10^{-4} mol dm^{-3}): λ_{max}/nm 334 (ε/dm^3 mol^{-1} cm^{-1} 27 900), 506 (4000). ^{1}H NMR (400 MHz, Me_2CO-d_6) δH/ppm 9.81 (1H, s, H3), 8.80 (1H, d, J = 8, H3′), 8.71 (1H, br d, H6), 8.31 (1H, br t, H4′), 7.74–7.66 (3H, m, H5′/H8/H7), 2.70 (3H, s, Me of quinoline ring), 2.12 (3H, s, Me of pyridine ring overlaped with the residual protons of Me_2CO-d_6). ^{13}C{^{1}H} NMR (100 MHz, Me_2CO-d_6) δC/ppm 166.52 (COOH), 158.76 (C6′), 154.34 (C2), 153.13 (C2′), 147.46 (C10), 140.56 (C4′), 139.12 (C4), 137.04 (C9), 133.91 (C8), 129.90 (C7), 127.82 (C5′), 125.41(C5), 124.93 (C6), 122.84 (C3′), 122.20 (C3), 24.36 (Me of pyridine ring), 19.46 (Me of quinoline ring).

Synthesis of [Cu(dmdcbpy)$_2$][PF$_6$]·3DMSO (5·3DMSO)

In a Schlenk tube, 18 mg (0.066 mmol) of dmdcbpy was dissolved in warm DMSO (5 mL) and then [Cu(MeCN)$_4$][PF$_6$] (12 mg, 0.033 mmol) was added. The color of the solution turned to red, and the mixture was stirred at ambient temperature for about 1 h. The solvent was pumped down under reduced pressure and a mixture of acetone/diethyl ether was added (1/20, v/v) to afford a dark red solid. The solid was filtered, washed once with a mixture of acetone/diethyl ether (1/30, v/v) and dried under vacuum at ambient temperature for 24 h. Yield: (0.024 g, 75%). The spectroscopic data of **5** are in accordance with those reported in the literature.[13]

General synthesis of copper(I) complexes 6–8

A Schlenk tube was charged with two molar equivalents of the methyl ester analogue **6′-Mepqca** (**8-Mepqca** or **8,6′-Me$_2$pqca**) and one equivalent of [Cu(MeCN)$_4$][PF$_6$], and the solids were degassed under vacuum for 10 minutes. Dry CH_2Cl_2 (10 mL) was then added, and the reaction mixture was stirred at ambient temperature for 1.5 h. Subsequently, the solvent was evaporated to dryness; the residue washed with diethyl ether (4 × 7 mL) and pentane (2 × 7 mL) and was dried under vacuum for 24 h, affording compounds **6–8** as analytically pure solids.

[Cu(6′-Mepqcame)$_2$][PF$_6$] (6). 6′-Mepqcame (73 mg, 0.27 mmol) and [Cu(MeCN)$_4$][PF$_6$] (50 mg, 0.135 mmol). Purple solid. Yield: (0.093 g, 90%). Decomp. >222 °C. Found: C, 53.4; H, 3.9; N, 7.2. $C_{34}H_{28}CuF_6N_4O_4P{\cdot}0.1(C_5H_{12}H21HH){\cdot}0.1(H_2O)$ requires C, 53.5; H, 3.8; N, 7.2%. IR (KBr, ν_{max}/cm^{-1}): 3096 (m, ν(C–H)$_{arom}$), 2953 (m, ν_{as}(C–H)$_{aliph}$), 2925 (m, ν_{as}(C–H)$_{aliph}$), 2853 (w, ν_s(C–H)$_{aliph}$), 1729 (s, ν_{as}(C=O)), 1600 (s, ν(C=C)), 1571 (m, ν(C=C)), 1473 (s, ν(C=N)), 1252 (s, ν_s(C–O)), 1147 (m, ν_{as}(O–CH_3)), 840 (vs, ν_3(P–F)), 794 (s, γ(C–H)$_{out\text{-}of\text{-}plane}$), 775 (s, γ(C–H)$_{out\text{-}of\text{-}plane}$), 558 (s, ν_4(P–F)). UV-vis (Me_2CO, 1.0 × 10^{-4} mol dm^{-3}): λ_{max}/nm 333 (ε/dm^3 mol^{-1} cm^{-1} 40 200), 532 (9900). ^{1}H NMR (500 MHz, $CDCl_3$) δH/ppm 9.05 (1H, s, H3), 8.88 (1H, br s, H9), 8.62 (1H, br s, H3′), 8.19 (1H, br s, H4′), 7.77 (1H, br s, H6), 7.65 (1H, br s, H8), 7.55 (1H, br s, H5′), 7.49 (2H, t, J = 10, H7), 4.21 (3H, s, COOMe), 2.15 (3H, s, Me). ^{13}C{^{1}H} NMR (126 MHz, $CDCl_3$) δC/ppm 165.86 (*C*OOMe), 158.11 (C6′), 152.15 (C2), 150.88 (C2′), 146.35 (C10), 139.45 (C4′), 137.27 (C4), 131.85 (C7), 130.24 (C8), 128.40 (C6), 127.59 (C5′), 126.81 (C5), 126.36 (C9), 121.37 (C3′), 120.97 (C3), 53.58 (COOMe), 25.21 (Me of pyridine ring). ESI-MS (MeOH, positive mode): m/z 619.14 [M–PF_6]$^+$ (calc. 619.14, base peak).

[Cu(8-Mepqcame)$_2$][PF$_6$] (7). 8-Mepqcame (100 mg, 0.36 mmol) and [Cu(MeCN)$_4$][PF$_6$] (67 mg, 0.18 mmol). Black-purple solid. Yield: (0.125 g, 95%). Decomp. >138 °C. Found: C, 53.9; H, 4.1; N, 7.2. $C_{34}H_{28}CuF_6N_4O_4P{\cdot}0.1(C_5H_{12}){\cdot}0.1(C_4H_{10}O)$ requires C, 53.8; H, 3.9; N, 7.2%. IR (KBr, ν_{max}/cm^{-1}): 3080 (m, ν(C–H)$_{arom}$), 2954 (m, ν_{as}(C–H)$_{aliph}$), 2923 (m, ν_{as}(C–H)$_{aliph}$), 2849 (w, ν_s(C–H)$_{aliph}$), 1727 (s, ν_{as}(C=O)), 1595 (s, ν(C=C)), 1548 (m, ν(C=C)), 1476

(s, ν(C=N)), 1263 (s, ν_s(C–O)), 1105 (m, ν_{as}(O–CH_3)), 841 (vs, ν_3(P–F)), 771 (s, γ(C–H)$_{out\text{-}of\text{-}plane}$), 764 (s, γ(C–H)$_{out\text{-}of\text{-}plane}$), 557 (s, ν_4(P–F)). UV-vis ($CHCl_3$, 1.0 × 10^{-4} mol dm^{-3}): λ_{max}/nm 338 (ε/dm^3 mol^{-1} cm^{-1} 22 700), 513 (2800). ^{1}H NMR (400 MHz, $CDCl_3$) δH/ppm 8.77 (1H, s, H3), 8.67 (1H, d, J = 8, H6), 8.55 (1H, d, J = 8, H3′), 8.17 (1H, t, J = 8, H4′), 7.96 (1H, br s, H6′), 7.57 (1H, t, J = 8, H7), 7.51–7.48 (2H, m, H8/H5′), 4.15 (3H, s, COOMe), 2.68 (3H, s, Me of pyridine ring). ^{13}C{^{1}H} NMR (100 MHz, $CDCl_3$) δC/ppm 166.07 (*C*OOMe), 152.85 (C2′), 152.50 (C2), 148.32 (C6′), 146.24 (C10), 139.15 (C4′), 137.83 (C4), 135.63 (C9), 133.13 (C8), 129.29 (C7), 126.87 (C5′), 126.68 (C5), 124.40 (C6), 124.11 (C3′), 120.58 (C3), 53.36 (COOMe), 19.19 (Me of quinoline ring).

[Cu(8,6′-Me_2pqcame)$_2$][PF_6] (8). 8,6′-Me_2pqcame (104 mg, 0.36 mmol) and [Cu(MeCN)$_4$][PF_6] (66 mg, 0.18 mmol). Red solid. Yield: (0.13 g, 96%). Decomp. >194 °C. Found: C, 54.1; H, 4.35; N, 6.9. $C_{36}H_{32}CuF_6N_4O_4P{\cdot}0.4H_2O$ requires C, 54.0; H, 4.1; N, 7.0%. IR (KBr, ν_{max}/cm^{-1}): 3087 (m, ν(C–H)$_{arom}$), 2956 (m, ν_{as}(C–H)$_{aliph}$), 2925 (m, ν_{as}(C–H)$_{aliph}$), 2851 (w, ν_s(C–H)$_{aliph}$), 1729 (s, ν_{as}(C=O)), 1601 (s, ν(C=C)), 1573 (m, ν(C=C)), 1472 (s, ν(C=N)), 1266 (s, ν_s(C–O)), 1113 (m, ν_{as}(O–CH_3)), 841 (vs, ν_3(P–F)), 773 (s, γ(C–H)$_{out\text{-}of\text{-}plane}$), 749 (s, γ(C–H)$_{out\text{-}of\text{-}plane}$), 557 (s, ν_4(P–F)). UV-vis ($CHCl_3$, 1.0 × 10^{-4} mol dm^{-3}): λ_{max}/nm 339 (ε/dm^3 mol^{-1} cm^{-1} 25 100), 513 (3950). ^{1}H NMR (400 MHz, $CDCl_3$) δH/ppm 8.81 (1H s, H3), 8.69 (1H, d, J = 8, H6), 8.46 (1H, d, J = 8, H3′), 8.14 (1H, t, J = 8, H4′), 7.58 (1H, t, J = 8, H7), 7.52–7.47 (2H, m, H8/H5′), 4.16 (3H, s, COOMe), 2.58 (3H, s, Me of quinoline ring), 1.94 (3H, s, Me of pyridine ring). ^{13}C{^{1}H} NMR ($CDCl_3$, 100 MHz, 298 K) δC/ppm 166.07 (*C*OOMe), 157.78 (C6′), 153.13 (C2), 151.97 (C2′), 146.42 (C10), 139.58 (C4′), 138.54 (C4), 135.59 (C9), 133.90 (C8), 129.38 (C7), 127.32 (C5′), 126.91 (C5), 124.76 (C6), 122.24 (C3′), 121.31 (C3), 53.58 (COOMe), 24.59 (Me of pyridine ring), 19.56 (Me of quinoline ring).

Crystallography

The data collection on **pqca** was performed on a Nonius KappaCCD diffractometer by using graphite monochromated Mo-K_α radiation (λ = 0.7103 Å), generated by a sealed tube. The data collection for **6′-Mepqca**, **1·DMSO**, 2{**2**·$Me_2CO{\cdot}0.5H_2O$}, **6**·$CHCl_3{\cdot}0.13H_2O$ was done using a Bruker D8 Venture diffractometer with Cu-K_α radiation (λ = 1.5418 Å) generated from an Ils Helios Optics source. For **8-Mepqca**, **4**, 2{**7**·C_5H_{12}}·$CHCl_3$ and **8**, a Bruker X8 Kappa ApexII diffractometer was used. The diffractometers were equipped with a low-temperature device (Bruker Kryoflex I, and Oxford Cryostream 800er series, both at 100(2) K). Intensities were measured by fine-slicing x and u-scans and corrected for background, polarization, and Lorentz effects.[71,72]

The structures were solved by intrinsic phasing methods implemented in Sheldrick's XT program and refined anisotropically by the least-squares procedure implemented in the SHELX program system.[72,73] Hydrogen atoms were included using the riding model on the bound carbon atoms. ORTEP-type diagrams and structure analysis used Mercury v. 3.0.

Crystallographic data and refinement conditions for compounds 1–4 are summarized below

Crystal structure determination of compound Pqca. Crystal data. $C_{15}H_{10}N_2O_2$, M = 250.25, clear colorless plate, monoclinic, space group $P2_1/n$, a = 15.6978(8), b = 3.70820(10), c = 19.3323(10) Å, U = 1106.76(9) Å^3, Z = 4, D_c = 1.502 g cm^{-3}, μ = 0.102 mm^{-1}, T = 123 K. Total 22 821 reflections, 2652 unique, R_{int} = 0.1397, Parameters = 173, Final R indexes [$I > 2\sigma(I)$] R_1 = 0.0765, Final R indexes [all data] wR_2 = 0.2094. CCDC 2184654.†

Crystal structure determination of compound 6′-Mepqca. Crystal data. $C_{16}H_{12}N_2O_2$, M = 264.28, clear colorless needle, orthorhombic, space group $P2_12_12_1$, a = 4.9065(3), b = 13.8542(8), c = 18.1645(11) Å, U = 1234.74(13) Å^3, Z = 4, D_c = 1.422 g cm^{-3}, μ = 0.778 mm^{-1}, T = 100 K. Total 18 142 reflections, 2230 unique, R_{int} = 0.0989, Parameters = 184, Final R indexes [$I > 2\sigma(I)$] R_1 = 0.0405, Final R indexes [all data] wR_2 = 0.0988. CCDC 2184655.†

Crystal structure determination of complex 1·DMSO. Crystal data. $C_{32}H_{26}N_4O_5SCuPF_6$, M = 787.14, clear pink plate, orthorhombic, space group *Ccce*, a = 15.8987(11), b = 24.7403(11), c = 16.4218(8) Å, U = 6459.3(6) Å^3, Z = 8, D_c = 1.619 g cm^{-3}, μ = 2.776 mm^{-1}, T = 100 K. Total 49 400 reflections, 2944 unique, R_{int} = 0.1041, Parameters = 234, Final R indexes [$I > \sigma(I)$] R_1 = 0.0538, Final R indexes [all data] wR_2 = 0.1432. CCDC 2184656.†

Crystal structure determination of complex 2 {2·$Me_2CO{\cdot}0.5H_2O$}. Crystal data. $C_{70}H_{62}Cu_2F_{12}N_8O_{11}P_2$, M = 1608.29, clear red plate, monoclinic, space group $P2_1$, a = 13.2628(7), b = 15.8514(8), c = 16.7898(9) Å, U = 3490.0(3) Å^3, Z = 2, D_c = 1.530 g cm^{-3}, μ = 2.048 mm^{-1}, T = 150 K. Total 56 596 reflections, 12 559 unique, R_{int} = 0.0738, Parameters = 1074, Final R indexes [$I > 2\sigma(I)$] R_1 = 0.0623, Final R indexes [all data] wR_2 = 0.1718. CCDC 2184657.†

Crystal structure determination of complex 6·$CHCl_3{\cdot}0.13H_2O$. Crystal data. $C_{35}H_{29.29}Cl_3CuF_6N_4O_{4.14}P$, M = 887.09, clear pink plate, monoclinic, space group $C2/c$, a = 31.4899(10), b = 9.7925(3), c = 27.9839(10) Å, U = 7585.7(4) Å^3, Z = 8, D_c = 1.554 g cm^{-3}, μ = 3.815 mm^{-1}, T = 100 K. Total 69 447 reflections, 6873 unique, R_{int} = 0.1200, Parameters = 532, Final R indexes [$I > 2\sigma(I)$] R_1 = 0.0964, Final R indexes [all data] wR_2 = 0.2710. CCDC 2184658.†

Crystal structure determination of complex 2 {7·C_5H_{12}}·$CHCl_3$. Crystal data. $C_{79}H_{81}Cl_3Cu_2F_{12}N_8O_8P_2$, M = 1793.88, clear dark violet plate, triclinic, space group $P\bar{1}$, a = 14.8494(11), b = 16.0090(13), c = 18.9006(13) Å, U = 3934.8(5) Å^3, Z = 2, D_c = 1.514 g cm^{-3}, μ = 0.773 mm^{-1}, T = 100 K. Total 89 442 reflections, 18 851 unique, R_{int} = 0.2108, Parameters = 1122, Final R indexes [$I > 2\sigma(I)$] R_1 = 0.0906, Final R indexes [all data] wR_2 = 0.2781. CCDC 2184659.†

Crystal structure determination of complex 8. Crystal data. $C_{36}H_{32}N_4O_4F_6PCu$, M = 793.16, clear red plate, monoclinic, space group $P2_1/c$, a = 11.4400(11), b = 13.1744(13), c = 22.711(2) Å, U = 3368.6(6) Å^3, Z = 4, D_c = 1.564 g cm^{-3}, μ = 0.777 mm^{-1}, T = 100 K. Total 63 827 reflections, 8115 unique,

R_{int} = 0.0880, Parameters = 475, Final R indexes [$I > 2\sigma(I)$] R_1 = 0.0436, Final R indexes [all data] wR_2 = 0.1497. CCDC 2184660.†

Solar cell fabrication. Photoanodes of 12 μm thickness were fabricated by commercial titania pastes (Greatcell Solar) that differ in the size of the titania nanoparticles: the NRAO active opaque paste with active (20 nm) and scatter nanoparticles (up to 450 nm) and the WER4 reflector paste that contains scatter nanoparticles (250–350 nm). FTO glass (TEC-8, Dyesol) was thoroughly cleaned in an ultrasonic bath with a detergent solution, acetone, and ethanol, respectively. The best-performing DSSC, prior to the active titania layer, was treated with an aqueous solution of 40 mM $TiCl_4$ (30 min at 70 °C – procedure repeated twice) as a compact layer (CL). Then, a layer of the NRAO paste followed. The films were annealed at 125 °C (5 min), 325 °C (15 min) and 525 °C (30 min). A second layer of the WER4 paste was deposited by the doctor blade technique and the films were annealed repeatedly. Respectively, for the triple-layered photoanodes, the DSL (Greatcell Solar) transparent titania paste was firstly applied onto the FTO substrates prior to the use of the following layers of the NRAO and WER4 titania pastes. Finally, the films were immersed in a 40 mM $TiCl_4$ solution (70 °C for 60 min) and were re-annealed at 450 °C for 60 min. The films were sensitised by being immersed overnight in copper-based dye solutions of approximately 1.2×10^{-4} M in Me_2CO (MeOH for **5**). After this period, the sensitized photoanodes were removed from the reaction medium and washed thoroughly with acetone. A drop of the liquid electrolyte: 1,3-dimethylimidazolium iodide (1M), lithium iodide (50 mM), iodine (15 mM), 4-*tert*-butylpyridine (0.5M) and guanidinium thiocyanate (0.1M) in a mixture of acetonitrile and butyronitrile (volume ratio 85 : 15) was cast upon the sensitized film (photoanode). Sputtered platinum on FTO glass was used as a counterelectrode. The active area of the DSSCs was set to 0.25 cm^2.

The DSSCs were illuminated under simulated solar light (1 sun, 1000 W m^{-2}) from a 300 W, Xe source in combination with AM 1.5G optical filters (Oriel). The active area was set at 0.152 cm^2, using a large black mask in front of the cells. Current density–voltage (J–V) measurements (under dark and light conditions) were recorded using linear sweep voltammetry on an Autolab PGSTAT30 potentiostat, working in a two-electrode mode, at a scan rate of 20 mV s^{-1}.

Conclusions

In this paper, a series of new sterically demanding pyridine-quinoline ligands has been reported. These compounds were specially tailored to sterically protect the copper(I) metal centre of the homoleptic complexes **1–4** and **6–8**, with carboxylic acid and methyl ester groups respectively in their periphery. Methyl substitution at the 6′ position efficiently protects the copper metal centre as indicated by the increased stability of **2** (36 days in acetone solution), checked by ^{1}H NMR spectroscopy, compared with the non-substituted analogue **1** (14 days). The new copper(I) complexes have been applied as photosensitizers in DSSCs.

Chemisorption of complexes **1**, **2** onto the TiO_2 surface became apparent by UV-vis and FT-IR spectroscopy, while the surface characteristics of dye **2** sensitized films were studied by Raman spectroscopy, implying weak electronic coupling of **2** onto the semiconductor surface. The photovoltaic performances of solar cell devices gave efficiencies ranging from 0.1% to 1.20%, while complexes with methyl esters did not perform efficiently as photosensitizers in DSSCs. After optimization of the photoanodes, a combination of dye **2** and a three-component anode (compact layer/opaque layer/scattering layer) afforded an overall conversion of η = 1.20%, higher than that of the **5**-cell reference, which in our hands showed η = 1.05%. As a result, the **2**-based device may be considered as a promising candidate, appropriate for cost-efficient building-integrated outdoor applications in DSSCs. Based on these results, the judicious design and development of some new copper(I) based molecular antennas is underway, rendering them candidates for the fabrication of highly performing photovoltaic devices based on DSSC technology.

Author contributions

Anastasios Peppas: investigation; formal analysis; writing – original draft. Demetrios Sokalis: investigation; formal analysis; Dorothea Perganti: investigation; formal analysis; Gregor Schnakenburg: resources; Polycarpos Falaras: supervision; resources; Athanassios I. Philippopoulos: conceptualization; funding acquisition; writing – review & editing; supervision.

Conflicts of interest

There are no conflicts to declare.

Acknowledgements

A. I. Philippopoulos would like to thank Prof. Dr A. C. Filippou of the Chemistry Department of the University of Bonn for the elemental analyses and Mrs Charlotte Rödde from the X-ray Department of the same Institute. Dr A. Peppas would like to thank the University of Bonn for financial support within the programme entitled: "Forschungs stipendium aus Mitteln des Sonder forschungs bereichs (SFB) 813 "Chemie an Spinzentren". This research work was supported by the Hellenic Foundation for Research and Innovation (HFRI) and the General Secretariat for Research and Technology (GSRT), under the HFRI PhD Fellowship grant (GA. no. 2055/14475 for the Ph.D. candidate A. Peppas). This research has also been co-financed in part by the Greek national funds through the Operational Program "Education and Lifelong Learning" of the National Strategic Reference Framework (NSRF)-Research Funding Program: THALES, investing in knowledge society through the European Social Fund. Project title: "Innovative

materials for nanocrystalline solar cells" (MIS: 377756). P. Falaras acknowledges co-financing of this research by the European Regional Development Fund of the European Union and Greek national funds through the Operational Program Competitiveness, Entrepreneurship and Innovation, under the call RESEARCH – CREATE – INNOVATE (project code:T1EDK-03547, MIS 5033808).

References

1 B. O'Regan and M. Grätzel, *Nature*, 1991, **353**, 73.
2 M. Grätzel, *J. Photochem. Photobiol., A*, 2004, **164**, 3.
3 S. Mathew, A. Yella, P. Gao, R. Humphry-Baker, B. F. E. Curchod, N. Ashari-Astani, I. Tavernelli, U. Rothlisberger, Md. K. Nazeeruddin and M. Grätzel, *Nat. Chem.*, 2014, **6**, 242.
4 A. Yella, H.-W. Lee, H. N. Tsao, C. Yi, A. K. Chandiran, Md. K. Nazeeruddin, E. W.-G. Diau, C.-Y. Yeh, S. M. Zakeeruddin and M. Grätzel, *Science*, 2011, **334**, 629.
5 K. Kakiage, Y. Aoyama, T. Yano, K. Oya, J. Fujisawab and M. Hanaya, *Chem. Commun.*, 2015, **51**, 15894.
6 T. Bessho, S. M. Zakeeruddin, C.-Y. Yeh, E. W.-G. Diau and M. Grätzel, *Angew. Chem., Int. Ed.*, 2010, **49**, 664.
7 S. Gauthier, B. Caro, F. Robin-Le Guen, N. Bhuvanesh, J. A. Gladysz, L. Wojcik, N. Le Poul, A. Planchat, Y. Pellegrin, E. Blart, D. Jacquemin and F. Odobel, *Dalton Trans.*, 2014, **43**, 11233.
8 G. C. Vougioukalakis, A. I. Philippopoulos, T. Stergiopoulos and P. Falaras, *Coord. Chem. Rev.*, 2011, **255**, 2602.
9 C. E. Housecroft and E. C. Constable, *Chem. Soc. Rev.*, 2015, **44**, 8386.
10 N. Robertson, *ChemSusChem*, 2008, **1**, 977.
11 N. Alonso-Vante, J.-F. Nierengarten and J.-P. Sauvage, *J. Chem. Soc., Dalton Trans.*, 1994, 1649.
12 T. Bessho, E. C. Constable, M. Graetzel, A. Hernandez Redondo, C. E. Housecroft, W. Kylberg, M. K. Nazeeruddin, M. Neuburger and S. Schaffner, *Chem. Commun.*, 2008, 3717.
13 (*a*) E. C. Constable, A. H. Redondo, C. E. Housecroft, M. Neuburger and S. Schaffner, *Dalton Trans.*, 2009, 6634; (*b*) B. Bozic-Weber, E. C. Constable and C. E. Housecroft, *Coord. Chem. Rev.*, 2013, **257**, 3089.
14 N. Armaroli, G. Accorsi, F. Cardinali and A. Listorti, *Top. Curr. Chem.*, 2007, **280**, 69.
15 A. K. Ichinaga, J. R. Kirchhoff, D. R. McMillin, C. O. Dietrich-Buchecker, P. A. Marnot and J. P. Sauvage, *Inorg. Chem.*, 1987, **26**, 4290.
16 B. Bozic-Weber, E. C. Constable, C. E. Housecroft, P. Kopecky, M. Neuburger and J. A. Zampese, *Dalton Trans.*, 2011, **40**, 12584.
17 S. Y. Brauchli, F. J. Malzner, E. C. Constable and C. E. Housecroft, *RSC Adv.*, 2015, **5**, 48516.
18 F. J. Malzner, S. Y. Brauchli, E. C. Constable, C. E. Housecroft and M. Neuburger, *RSC Adv.*, 2014, **4**, 48712.
19 (*a*) E. Schönhofer, B. Bozic-Weber, C. J. Martin, E. C. Constable, C. E. Housecroft and J. A. Zampese, *Dyes Pigm.*, 2015, **115**, 154; (*b*) G. Risi, M. Becker, C. E. Housecroft and E. C. Constable, *Molecules*, 2020, **25**, 1528.
20 M. Sandroni, M. Kayanuma, A. Planchat, N. Szuwarski, E. Blart, Y. Pellegrin, C. Daniel, M. Boujtita and F. Odobel, *Dalton Trans.*, 2013, **42**, 10818.
21 (*a*) M. Sandroni, L. Favereau, A. Planchat, H. Akdas-Kilig, N. Szuwarski, Y. Pellegrin, E. Blart, H. Le Bozec, M. Boujtita and F. Odobel, *J. Mater. Chem. A*, 2014, **2**, 994; (*b*) M. S. Yann Pellegrin, E. Blart, A. Planchat, M. Evain, N. C. Bera, M. Kayanuma, M. Sliwa, M. Rebarz, O. Poizat, C. Daniel and F. Odobel, *Inorg. Chem.*, 2011, **50**, 11273.
22 Y. Liu, S.-C. Yiu, C.-L. Ho and W.-Y. Wong, *Coord Chem Rev*, 2018, **375**, 514.
23 (*a*) B. N. Mongal, A. Pal, T. K. Mandal, J. Datta and S. Naskar, *Polyhedron*, 2015, **102**, 615; (*b*) K. A. Wills, H. J. Mandujano-Ramirez, G. Merino, D. Mattia, T. Hewat, N. Robertson, G. Oskam, M. D. Jones, S. E. Lewis and P. J. Cameron, *RSC Adv.*, 2013, **3**, 23361; (*c*) R. Ilmi, I. Juma Al-busaidi, A. Haque and M. S. Khan, *J. Coord. Chem.*, 2018, **71**, 3045.
24 E. Kolovou, A. Peppas, N. Zacharopoulos, K. Koukoulakis, E. Bakeas, G. Schnakenburg and A. I. Philippopoulos, *Inorg. Chem. Commun.*, 2018, **92**, 64.
25 A. Philippopoulos, E. Chatzivasiloglou, O. Igglessi-Markopoulou, V. Likodimos, G.-C. Konti and P. Falaras, *J. Coord. Chem.*, 2012, **65**, 2535.
26 G. Konti, E. Chatzivasiloglou, V. Likodimos, G. Kantonis, A. G. Kontos, A. I. Philippopoulos and P. Falaras, *Photochem. Photobiol. Sci.*, 2009, **8**, 726.
27 A. Peppas, E. Papadaki, G. Schnakenburg, V. Magrioti and A. I. Philippopoulos, *Polyhedron*, 2019, **171**, 412.
28 N. Zacharopoulos, E. Kolovou, A. Peppas, K. Koukoulakis, E. Bakeas, G. Schnakenburg and A. I. Philippopoulos, *Polyhedron*, 2018, **154**, 27.
29 D. M. Classen, *Inorg. Chem.*, 1976, **15**, 3166.
30 (*a*) A. Peppas *Synthesis and characterization of homoleptic Copper(I) complexes. Application in third generation solar cells (Gratzel type)*. Master thesis, National and Kapodistrian University of Athens, Greece, 2015. Persistent URL: **https://pergamos.lib.uoa.gr/uoa/dl/object/1320032**; (*b*) A. A. Farah, J. G. C. Veinot, M. Najman and W. J. Pietro, *Macromol. Sci., Pure Appl. Chem.*, 2000, **37**, 1507.
31 A. Peppas *"Synthesis and characterization of complexes of Cu (I) compounds for use in nanocrystalline solar cells"*. Doctoral Dissertation, National and Kapodistrian University of Athens, Athens, Greece, 2019. Persistent URL: **https://pergamos.lib.uoa.gr/uoa/dl/object/2884748**.
32 G. J. Atwell, B. C. Baguley and W. A. Denny, *J. Med. Chem.*, 1989, **32**, 396.
33 R. F. Fernandes, P. H. F. Stroppa, G. R. Ferreira, A. D. da Silva, H. G. M. Edwards and L. F. C. de Oliveira, *Vib. Spectrosc.*, 2016, **86**, 128.

34 A. A. Farah and W. J. Pietro, *Acta Crystallogr., Sect. E: Struct. Rep. Online*, 2001, **E57**, o677–o678.
35 C. Janiak, *J. Chem. Soc., Dalton Trans.*, 2000, 3885.
36 S. J. Grabowski, *Crystals*, 2016, **6**, 59.
37 (*a*) S. Sakaki, T. Kuroki and T. Hamada, *J. Chem. Soc., Dalton Trans.*, 2002, 1649; (*b*) A. Colombo, C. Dragonetti, D. Roberto, A. Valore, P. Biagini and F. Melchiorre, *Inorg. Chim. Acta*, 2013, **407**, 204.
38 A. Milton, F. Benial, V. Ramakrishnan and R. Murugesan, *Spectrochim. Acta, Part A*, 2002, **58**, 1703.
39 T. E. Hewat, J. Yellowlees and N. Robertson, *Dalton Trans.*, 2014, **43**, 4127.
40 L. Yang, D. R. Powell and R. P. Houser, *Dalton Trans.*, 2007, 955.
41 M. G. Fraser, H. van der Salm, S. A. Cameron, A. G. Blackman and K. C. Gordon, *Inorg. Chem.*, 2013, **52**, 2980.
42 S. Keller, M. Alkan-Zambada, A. Prescimone, E. C. Constable and C. E. Housecroft, *Crystals*, 2020, **10**, 255.
43 T. Steiner, *Crystallogr. Rev.*, 2003, **9**, 177.
44 N. Armaroli, *Chem. Soc. Rev.*, 2001, **30**, 113.
45 Y. Liu, S.-C. Yiu, C.-L. Ho and W.-Y. Wong, *Coord. Chem. Rev.*, 2018, **375**, 514.
46 M. W. Mara, K. A. Fransted and L. X. Chen, *Coord. Chem. Rev.*, 2015, **282–283**, 2.
47 A. I. Philippopoulos, A. Terzis, C. P. Raptopoulou, V. J. Catalano and P. Falaras, *Eur. J. Inorg. Chem.*, 2007, 5633.
48 B. Bozic-Weber, S. Y. Brauchli, E. C. Constable, S. O. Furer, C. E. Housecroft, F. J. Malzner, I. A. Wright and J. A. Zampese, *Dalton Trans.*, 2013, **42**, 12293.
49 J. W. Kee, Y. Y. Ng, S. A. Kulkarni, S. K. Muduli, K. Xu, R. Ganguly, Y. Lu, H. Hirao and H. S. Soo, *Inorg. Chem. Front.*, 2016, **3**, 651.
50 K. A. Wills, H. J. Mandujano-Ramirez, G. Merino, D. Mattia, T. Hewat, N. Robertson, G. Oskam, M. D. Jones, S. E. Lewis and P. J. Cameron, *RSC Adv.*, 2013, **3**, 23361.
51 G. Boschloo and A. Hagfeldt, *Acc. Chem. Res.*, 2009, **42**, 1819.
52 Y. Zhou, Q. He, Y. Yang, H. Zhong, C. He, G. Sang, W. Liu, C. Yang, F. Bai and Y. Li, *Adv. Funct. Mater.*, 2008, **18**, 3299.
53 J. Jiang, J. A. Spies, J. R. Swierk, A. J. Matula, K. P. Regan, N. Romano, B. J. Brennan, R. H. Crabtree, V. S. Batista, C. A. Schmuttenmaer and G. W. Brudvig, *J. Phys. Chem. C*, 2018, **122**, 13529.
54 A. Hagfeldt, G. Boschloo, L. Sun, L. Kloo and H. Pettersson, *Chem. Rev.*, 2010, **110**, 6595.
55 P. Falaras, *Sol. Energy Mater. Sol. Cells*, 1998, **53**, 163.
56 C. Deng, P. F. James and P. V. Wright, *J. Mater. Chem.*, 1998, **8**, 153.
57 G. C. Vougioukalakis, T. Stergiopoulos, A. G. Kontos, E. K. Pefkianakis, K. Papadopoulos and P. Falaras, *Dalton Trans.*, 2013, **42**, 6582.
58 L. Zhu, Z. Yulong, X. P. Lin, X. Q. Gu and Y. Qiang, *Superlattices Microstruct.*, 2014, **65**, 152.
59 A. Burke, S. Ito, H. Snaith, U. Bach, J. Kwiatkowski and M. Grätzel, *Nano Lett.*, 2008, **8**, 977.
60 J. He, A. Hagfeldt, S.-E. Lindquist, H. Grennberg, F. Korodi, L. Sun and B. Åkermark, *Langmuir*, 2001, **17**, 2743.
61 S. C. Pradhan, A. Hagfeldt and S. Soman, *J. Mater. Chem. A*, 2018, **6**, 22204.
62 A. Colombo, C. Dragonetti, D. Roberto and F. Fagnani, *Molecules*, 2021, **26**, 194.
63 G. J. Kubas, B. Monzyk and A. L. Crumblis, *Inorg. Synth.*, 2007, **28**, 68.
64 M. Y. Goikhman, I. V. Podeshvo, N. L. Loretsyan, T. D. Anan'eva, R. Y. Smyslov, T. N. Nekrasova, M. A. Smirnov, E. N. Popova and A. V. Yakimanskii, *Polym. Sci., Ser. B*, 2011, **53**, 89.
65 T. Sandmeyer, *Helv. Chim. Acta*, 1919, **2**, 234.
66 P. J. Montoya-Pelaez, Y.-S. Uh, C. Lata, M. P. Thompson, R. P. Lemieux and C. M. Crudden, *J. Org. Chem.*, 2006, **71**, 5921.
67 G. Black, E. Depp and B. B. Corson, *J. Org. Chem.*, 1949, **14**, 14.
68 F. J. McCarty, C. H. Tilford and M. G. Van Campen, *J. Am. Chem. Soc.*, 1957, **79**, 472.
69 H. B. Amin and R. Taylor, *J. Chem. Soc., Perkin Trans. 1*, 1979, **2**, 624.
70 V.-M. Mukkala and J. J. Kankare, *Helv. Chim. Acta*, 1992, **75**, 1578.
71 Bruker SADABS-2014/5 (Bruker AXS Karlsruhe; **2014**).
72 G. M. Sheldrick, *Acta Crystallogr.*, 2008, **3**, A71.
73 G. M. Sheldrick, *Acta Crystallogr.*, 2008, **3**, C71.